# RESEARCH MEMORANDUM

## DESIGN AND EXPERIMENTAL INVESTIGATION OF TRANSONIC TURBINE WITH SLIGHT NEGATIVE REACTION ACROSS ROTOR HUB

By Warner L. Stewart, Robert Y. Wong, and David G. Evans

Lewis Flight Propulsion Laboratory
Cleveland, Ohio



NATIONAL ADVISORY COMMITTEE
FOR AERONAUTICS

WASHINGTON
March 12, 1954

NATIONAL ADVISORY COMMITTEE FOR AERONAUTICS

RESEARCH MEMORANDUM

# DESIGN AND EXPERIMENTAL INVESTIGATION OF TRANSONIC TURBINE WITH SLIGHT NEGATIVE REACTION ACROSS ROTOR HUB

By Warner L. Stewart, Robert Y. Wong, and David G. Evans



## SUMMARY

The design and experimental investigation of a transonic turbine are presented herein. The turbine was designed for a rotor-hub entrance Mach number of unity and a slight over-all negative reaction across the hub. The maximum design rotor-blade-surface Mach number was limited to a value of 1.33. Because of the increased flow Mach number level, the design procedure used was on a quasi-three-dimensional basis.

The results of the experimental investigation indicated that the design point was obtained at a total efficiency of 0.85 with one point in efficiency lost in exit whirl. Design equivalent specific-work output occurred 3 percent below the turbine limiting-loading point. This checked closely with the value of 5 percent obtained theoretically with design conditions. Off-design operation appeared to be similar to that obtained for more conservative turbine designs. Surveys behind the stator and rotor at the design point indicated that the loss patterns were quite similar to those found in lower Mach number turbines.

From the experimental results it was concluded that, under the prescribed conditions of surface Mach number and reaction, transonic turbines can be operated with efficiencies of at least 0.85. The quasi-three-dimensional design procedure was found to be sufficiently rigorous that the design conditions, although critical from a limiting-loading standpoint, could be met.

## INTRODUCTION

A research program has been in progress at the NACA Lewis laboratory to study problems associated with obtaining compact turbines for use in turbojet engines. Reference 1 indicates that the turbine component can be considerably reduced in size by increasing the flow

Mach numbers through the turbine considerably above those currently used. This increase in flow Mach number would result in increased specific-work output and weight flow per unit frontal area which, in turn, would reduce the turbine size for a given application.

Considerable work has been done in the transonic compressor field, and results of these investigations (ref. 2, e.g.) have indicated that these transonic flow Mach numbers can be utilized in compressors with a resultant wide range of efficient performance. In view of these results, it was felt that properly designed turbines should also be capable of operating efficiently in the transonic region.



Therefore, as part of the turbine research program, the design and experimental investigation of a transonic turbine has been conducted to study the problems associated with obtaining efficient turbines for this range of flow Mach numbers. A transonic turbine is defined as one designed to utilize a rotor-hub entrance Mach number of approximately unity. Because of the limitations imposed upon the flow conditions out of the rotor as a result of the limiting-loading characteristics, the reaction across the hub of these high Mach number turbines can become very small, zero, or even highly negative. The transonic turbine investigated was designed for a slight amount of negative reaction.

Because the three-dimensional characteristics of the flow become especially important as the Mach number level through the turbine is increased, it was felt that the design of these high Mach number turbines must include the three dimensionality of the flow. Hence, one such procedure was developed and used in the design of the transonic turbine. A limiting blade-surface Mach number of 1.33 was also selected for this turbine design as normal shock losses corresponding to this value do not become excessive (see ref. 3).

This report presents a complete description of the quasi-three-dimensional procedure used in the design of the transonic turbine. Results of the experimental investigation of this turbine will also be presented to indicate the validity of the design procedure used and the efficiency obtained under the prescribed design reaction and surface Mach number conditions. These experimental results include the over-all performance of the turbine over a wide range of speeds and pressure ratios together with detailed surveys downstream of stator and rotor at approximately the design point.

## TURBINE DESIGN

### Design Requirements

The transonic turbine investigated was a 14-inch cold-air turbine with a constant hub-tip radius ratio of 0.7 (dictated by limitations imposed by the test apparatus). The design requirements were chosen

such that the midchannel critical velocity ratio $W/W_{cr}$ is constant and equal to unity at the rotor hub from station 3 to station 5. (All symbols are defined in appendix A.) This condition resulted in a slight over-all negative reaction across the rotor hub from station 3 to station 6 as will be discussed in the section Velocity Diagrams.

The design requirements selected to meet these conditions are:

| | |
|---|---|
| $\frac{\Delta h'}{\theta_{cr}}$, Btu/lb | 22.6 |
| $\epsilon \frac{w\sqrt{\theta_{cr}}}{\delta}$, lb/sec | 11.95 |
| $\frac{U_t}{\sqrt{\theta_{cr}}}$, ft/sec | 597 |

## Velocity Diagrams

The design velocity diagrams were constructed at the free-stream stations 0, 3, and 6 at the hub, mean, and tip sections to meet the design requirements and are based on the following assumptions:

(1) Free vortex flow

(2) Simple radial equilibrium

(3) A 3-percent total-pressure loss across the stator

(4) Efficiency of 0.88 based on total-pressure ratio used to obtain velocity diagrams at station 6

These velocity diagrams together with a sketch of a typical blade channel showing the station nomenclature used are shown in figure 1. Also included are velocity diagrams at stations 2 and 5 (just inside the blade trailing edge). These diagrams will be discussed later in this section.

As indicated by figure 1, the stator is choked from hub to tip with a very high stator-hub exit velocity $\left[(V/V_{cr})_3 = 1.295\right]$. The design turning at the stator hub and tip are 66.8° and 58.3°, respectively. The rotor-hub entrance critical velocity ratio $(W/W_{cr})_3$ is unity (which defines the transonic turbine) and there is a slight negative reaction across the rotor hub $\left[(W/W_{cr})_3 = 1.000 \text{ and } (W/W_{cr})_6 = 0.922\right]$. The design reaction (defined herein as ratio of inlet to exit static pressure) across the rotor at the hub for this turbine is 0.91. The

turning in the rotor varies from 96.7° at the hub to 71.7° at the tip. It can further be seen that approximately 10° of negative exit whirl is included in the design and occurs as a result of the design requirements. The design rating efficiency, based on the axial component of total-pressure ratio, is then approximately 0.87 or 1 point below the efficiency based on actual total-pressure ratio.

Velocity diagrams were also constructed for the three sections at stations 2 and 5 for use in the blade design and are based on the following assumptions:

(1) No change in the tangential component of velocity was assumed to occur between stations 2 and 3 for the stator and stations 5 and 6 for the rotor.

(2) Continuity with no total-pressure loss was assumed between stations 2 and 3 for the stator and stations 5 and 6 for the rotor.

In the stator calculations, a trailing-edge blockage corresponding to 32 blades with a trailing-edge thickness of 0.030 inch was used. The calculations for station 5 were made for a trailing-edge blockage corresponding to 29 rotor blades and a trailing-edge thickness of 0.050 inch. In the subsequent blade design, as the number of blades was varied, the trailing-edge thickness was also changed such that the trailing-edge blockage remained constant, and thus the velocity diagram remained unchanged.

As shown in figure 1, the relative critical velocity ratio at station 5 is unity at the rotor hub. As discussed previously in the section Design Requirements, this is designed to occur. The axial component of the critical velocity ratio at the mean section at this station is also seen to be 0.782. As indicated by reference 4, this high value results in the turbine design point being extremely close to the limiting-loading point, in this case approximately 5 percent below. Thus the turbine design will be extremely critical from this standpoint.

## Stator Design

In the stator-blade design, 32 blades were used with a leading-edge radius of 0.075 inch and a trailing-edge radius of 0.015 inch. The blade sections were laid out at the three radial stations by using the velocity diagrams at station 2 in figure 1. For the tip section the throat dimension was obtained from the relation $o = (s_2 - t_2) \sin \alpha_2$ as the critical velocity ratio at station 2 was slightly subsonic. The

throat dimensions for the mean and hub sections were obtained from the relation $o = (s_2 - t_2)(\sin \alpha_2)(A_{cr}/A)_2$, where $(A_{cr}/A)_2$ is the critical area ratio corresponding to the supersonic critical velocity $(V/V_{cr})_2$. Straight-line suction surfaces were used for all three sections from the trailing edge to the throat. A smooth converging channel was used from the inlet to the throat with zero leading-edge incidence angle.

The three stator-blade sections were stacked such that the center of the trailing-edge circles lay in a radial line and the blade was then faired between the three sections. The resulting solidities at the hub and tip were approximately 1.9 and 1.7, respectively. Table I shows the coordinates of the stator sections, and figure 2 shows the sketch of the stator sections and flow passages.

3178

## Rotor Design

In the design of turbine rotors, it is important that surface Mach numbers be predicted accurately so that static-pressure gradients can be controlled. As the flow Mach numbers through the turbine rotor are increased into the transonic region, surface velocities can increase well into the supersonic range. Because of the potentially greater losses associated with supersonic surface velocities, it is even more important that these velocities be accurately predicted. The problem of predicting flow Mach numbers in the transonic and supersonic regions is complicated by the fact that the flow becomes extremely sensitive to the small area changes resulting from the radial shifts in the streamlines. Hence, the three-dimensional characteristics of the flow have an increasing significance as the flow Mach number is increased. Recent experience in the investigation of turbines for driving supersonic compressors (refs. 5 and 6, e.g.) also indicates the necessity of including provision for the three-dimensional effects of the flow in the design of choked rotor turbines. In view of these considerations, it is indicated that the design procedure of a turbine to operate in the transonic region should then be on a three-dimensional basis.

A three-dimensional design procedure was developed and used in the design of the transonic turbine rotor. In this design procedure, continuity across the rotor was satisfied and equilibrium in the radial-axial plane and across the channel from suction to pressure surface was also satisfied. Since these quantities were varied independently until all conditions were satisfied, the design procedure is necessarily an iteration process.

Design conditions and assumptions. - The following conditions and assumptions were made in the design of the transonic turbine rotor:

(1) Simple radial equilibrium was assumed to exist in the radial-axial plane from hub to tip at a series of stations from the rotor entrance to the rotor exit. Because a fairly long rotor-blade chord was used, it was felt that the term involving the curvature of the streamlines in the axial-radial plane could be ignored in the radial equilibrium calculations, thus permitting use of the simple radial equilibrium assumption. The axially symmetric or midchannel velocity distribution was calculated on this basis.

(2) The rotor-hub midchannel critical velocity ratio was specified to be constant and equal to unity from station 3 to station 5.



(3) The rotor total-pressure loss was assumed to vary linearly from station 3 to station 5.

(4) The maximum suction-surface critical velocity ratio was limited to a value of 1.25 (corresponding to a Mach number of 1.33).

(5) A zero blade incidence angle was assumed with a sharp leading edge. After the blade design was completed, the leading edge was rounded off to a radius of 0.015 inch (resulting in an angle of incidence of approximately $4^{\circ}$).

General design procedure. - The general procedure used in obtaining the rotor-blade shape is described in the following steps. A subsequent section presents the design of the transonic turbine rotor.

(1) At the mean and tip sections a midchannel velocity distribution between stations 3 and 5 was tentatively assumed with the hub midchannel critical velocity ratio specified in accordance with condition (2) of the preceding section.

(2) A rotor solidity was tentatively assumed.

(3) A blade shape was then obtained as follows (refer to fig. 3):

(a) A straight suction surface up to the channel inlet was set at the flow inlet angle $\beta_3$.

(b) A straight suction surface from the trailing edge to the channel exit was set at the flow exit angle $\beta_5$.

(c) The channel was then drawn such that for the assumed midchannel velocity distribution the surface velocity distribution was deemed to be satisfactory. The procedure used in obtaining the surface velocities is presented in appendix B. If the maximum surface velocity is then above the specified limit, the solidity will have to be changed and the process repeated. Thus at the three radii the blade sections were determined and a blade shape evolved.

(4) The blade shape was then analyzed to obtain the midchannel velocity distribution that must exist to satisfy simple radial equilibrium conditions. The procedure used to obtain this variation of the midchannel velocity for the given hub velocity distribution is also discussed in appendix B.

(5) The midchannel velocity distribution calculated in step (4) was then used to recompute the surface velocity distribution. If the surface velocities thus calculated are above the prescribed limits, the design steps beginning with step (2) are then repeated with the use of the calculated midchannel velocity distribution (step (4)) until a satisfactory shape is evolved from a velocity-distribution standpoint.



(6) The weight flow is then calculated from inlet to exit by using the blade shape obtained in step (5), as also described in appendix B. If the weight flow differs appreciably (over 1 percent for this design) from the design value, the flow area is altered proportionately and the preceding outlined steps repeated until the blade shape is satisfactory from both the surface-velocity and the weight-flow standpoints.

Transonic rotor-blade design. - A total of three trials with the procedure just outlined was made before a satisfactory rotor blade was evolved. A discussion of these trials is now presented.

Trial 1: A sinusoidal variation in the midchannel velocity distribution was first assumed from inlet to outlet at the mean and tip sections (step (1)). The hub midchannel critical velocity ratio was specified constant at a value of unity. The solidity was selected by assuming 29 blades with an axial chord of 3.2 inches (step (2)). A rotor-blade shape was then obtained (step (3)). With the assumed midchannel velocity distribution and solidity, the maximum surface velocity was within the prescribed limits and occurred at the rotor hub. The blade was then analyzed (step (4)), and it was found that the assumed and the calculated midchannel velocity distributions were in considerable disagreement and the resulting maximum surface velocity from the calculated midchannel velocity distribution was considerably above the limit (step (5)).

Trial 2: The midchannel velocity distribution obtained in trail 1 (step (4)) was used in step (1) of trial 2. The solidity was increased by increasing the number of blades to 35 (step (2)). A second blade shape was then evolved (step (3)); and it was found that with this solidity the maximum surface velocity was within the prescribed limit, but the maximum occurred at the tip section. The blade was then analyzed (step (4)), and it was found that the calculated midchannel velocity distribution differed only slightly from that calculated in the first trial.

The surface velocity from the calculated midchannel velocities was still found to be within the prescribed limits (step (5)). However, when the weight flow was calculated at the axial stations (step (6)), it was found that at some axial stations the calculated weight flow differed by as much as 6 percent from the design value.

Trial 3: The flow area at each axial station was altered by the ratio of the weight flow calculated in trial 2 to the design weight flow by means of adjusting the blade thickness. The area adjustment was made such that the mean camber angle remained the same and hence the midchannel velocity distribution would remain unchanged. The steps were repeated, and the surface velocities were found to be within the prescribed limits and the weight flow checked within 1 percent across the rotor. The rotor-blade design was then considered to be complete.



The rotor blade was formed by stacking the trailing edge of each section at the same axial station, and the centroids of each section lay in a common radial-axial plane. As discussed in the design assumptions, the sharp leading edge used in the design was rounded off to a 0.015-inch radius. Table II presents the rotor-blade coordinates.

Discussion of transonic turbine-rotor design. - The rotor-blade sections forming the flow passages at the hub, mean, and tip are shown in figure 2. At the hub, the channel is seen to diverge from the inlet to the exit, whereas at the mean section approximately constant channel width exists. At the tip section the channel is seen to converge rapidly from the inlet to the midchord and remains fairly constant to the exit. These channel variations occur as a result of considering the three-dimensional aspects of the flow in the design procedure in conjunction with the prescribed hub conditions. As stated previously in the section Transonic rotor-blade design, 35 blades were required in order to satisfy the surface velocity limitations imposed. This resulted in the hub and tip solidities of 3.5 and 2.5, respectively. These high solidities can be noted in figure 2.

The design midchannel and surface velocity distributions of the hub, mean, and tip sections are shown in figure 4. Constant midchannel critical velocity ratio at the hub is indicated. At the mean and tip sections, the midchannel velocity is seen to accelerate very rapidly from the inlet to the midchord and remains approximately constant thereafter. This condition stems from the specified hub conditions and from satisfying equilibrium requirements in the design procedure. Because of the rapid acceleration at the tip section, the maximum surface velocity was found to be at this section. It should be noted that the difference between the maximum surface critical velocity ratio and the outlet critical velocity ratio divided by the maximum surface critical velocity ratio, hereinafter referred to as diffusion, is approximately a constant value of 0.15 from hub to tip.

In figure 5 is shown the midchannel streamline and velocity variations across the rotor obtained in the final design. It can be seen that a line corresponding to a critical velocity ratio of unity crosses the rotor from hub to tip at approximately midchord position, indicating that the rotor obtained in the three-dimensional design choked approximately midway between the inlet and the exit. This condition was not felt to be critical as very little increase in velocity downstream from this point is designed to occur.

Comparison of three- and two-dimensional design procedures. - In order to emphasize the critical nature of designing turbines to operate in the transonic range, an analysis with an assumption common in two-dimensional design procedures was made on the final hub-section blade profile. This assumption as suggested in reference 7 is that a linear variation of the weight flow per unit height from entrance to exit of the rotor passage exists. The results of this analysis are shown in figure 6, and for comparison the midchannel critical velocity ratio distribution as specified in the three-dimensional design is also shown. It can be seen from the figure that the assumption of linear variation in weight flow per unit height resulted in insufficient flow area over the first half of the blade chord, thus yielding no solution. In the remaining half of the passage, a solution was obtained; however, there is no similarity between the critical velocity ratio distribution obtained from the two- and three-dimensional solutions. It is evident that entirely different blade sections would have been obtained had the two-dimensional design procedure been used. The results of this analysis further emphasize that turbines designed to operate in the transonic region should be designed on a three-dimensional basis in order that the velocity distributions be more accurately predicted.

## APPARATUS

The apparatus used in this investigation consisted primarily of the turbine configuration, suitable housing to give uniform turbine-inlet flow conditions, and a dynamometer which was coupled to the rotor through a speed-reducing gear box and a torquemeter shaft. A diagrammatic sketch of the turbine test section is shown in figure 7.

Dry pressurized air from the laboratory combustion air supply was brought to the collector (fig. 7) by means of inlet ducting which is not shown. In this ducting were placed an adjustable orifice for metering the flow, butterfly throttle valves to control the inlet pressure, and a filter tank for minimizing instrument failure and blade-surface erosion from foreign particles being carried along by the flow. The air leaving the turbine is exhausted through butterfly throttles which are used to control the exhaust pressure to the laboratory altitude exhaust system.

The 32 stator blades and the 35 rotor blades were machined from an aluminum alloy and were hand finished. The rotor-tip diameter was 13.94 inches, thus giving a rotor-tip clearance of 0.030 inch. A photograph of the turbine-rotor assembly is presented in figure 8, in which the high solidity of the blades can be noted.

## INSTRUMENTATION



Instrumentation was provided on the turbine apparatus to obtain a complete turbine performance map and blade-element performance over approximately one stator pitch for both the stator and the rotor.

Turbine performance instrumentation. - Air weight-flow measurements were made with a standard adjustable submerged orifice installed with long straight sections of ducting on either side and calibrated after installation. The torque output of the rotor was measured by the use of a strain-gage torquemeter (fig. 7), which is similar to that described in reference 8. Turbine speed was measured by use of an electronic tachometer in conjunction with a magnetic pickup and a ten-tooth sprocket gear mounted on the rotor shaft.

Turbine-inlet measurements were taken in the annulus upstream of the nozzle inlet (station 0, fig. 7). Four static-pressure taps were installed on each of the outer and inner walls and placed on four radial lines 90° apart. A thermocouple rake with five bare-wire thermocouples placed at centers of equal-annular areas was mounted in the same plane as the static taps.

Stator-outlet static pressures were measured from four static-pressure taps spaced approximately 90° apart on each of the inner and outer walls immediately downstream of the nozzle blades (station 3, fig. 7). Each pressure tap was centrally located in the projected nozzle-flow passage.

All turbine-outlet measurements were taken in the annulus downstream of the rotor outlet (station 6, fig. 7) with the exception of turbine-discharge temperature, which was taken further downstream. Absolute rotor-discharge flow angles were measured with a total-pressure claw probe mounted in a self-alining actuator. Four static-pressure taps were installed on each inner and outer wall and were spaced 90° apart. The turbine-discharge total temperature was measured in the discharge ducting approximately 4 feet downstream from the rotor (station not shown in fig. 7) with a thermocouple rake which consisted of five doubly shielded thermocouples placed at centers of equal-annular areas. The turbine casing between the rotor and the measuring station was insulated with 2 inches of glass wool in order to minimize heat transfer. Both the inlet and the discharge total-temperature rakes were calibrated for recovery factor over the range of Mach numbers encountered.

Blade-element performance instrumentation. - Radial and circumferential surveys of total pressure were made at the stator and rotor exit (stations 3 and 6, fig. 7) with a miniature claw mounted in a self-alining actuator that could move the probe not only radially but also circumferentially. Total-pressure variations were transmitted to an X-Y recorder through a pressure transducer and recorded against circumferential travel of the probe. Radial and circumferential surveys of total temperature were taken at the rotor exit in a manner similar to that just described.



## EXPERIMENTAL PROCEDURE

The experimental investigation was conducted by operating the turbine at constant nominal inlet conditions of 32 inches mercury absolute and 145° F and at constant speed values over a range from 30 to 130 percent of design speed in even increments of 10 percent. For each speed investigated, a range of total-pressure ratios from approximately 1.4 to that corresponding to limiting loading was obtained.



Detailed circumferential and radial surveys of total temperature and total pressure were made downstream of the rotor (station 6) at design speed and a work output of approximately design. Detailed circumferential and radial surveys of total pressure downstream of the stator (station 3) were also made for the same condition.

## CALCULATIONS

The turbine was rated on the basis of the ratio of the inlet total pressure to the rotor discharge total pressure, which is defined as the sum of the static pressure and the axial component of the turbine discharge velocity at that station. The inlet total pressure was calculated from the weight flow, inlet static pressure, and inlet total temperature by the following equation, which is a rearranged form of equation 2 of reference 5:

$$\frac{w\sqrt{T_0'}}{p_0' A_a} = \left[\frac{2\gamma g}{(\gamma - 1)R}\right]^{\frac{1}{2}} \left\{\left[\left(\frac{p_0'}{p_0}\right)^{\frac{\gamma-1}{\gamma}} - 1\right] + \left[\left(\frac{p_0'}{p_0}\right)^{\frac{\gamma-1}{\gamma}} - 1\right]^2\right\}^{\frac{1}{2}}$$

The outlet total pressure which was defined as the sum of the static pressure and the axial component of the discharge velocity head was

[redacted]

calculated from the following equation, which is a rearranged form of equation 3 of reference 5:

$$\frac{w\sqrt{T_7'}}{p_6' A_a} = \left[\frac{2g\gamma}{(\gamma - 1)R}\right]^{\frac{1}{2}} \left\{\left[\left(\frac{p_6'}{p_6}\right)^{\frac{\gamma-1}{\gamma}} - 1\right] + \left[\frac{\left(\frac{p_6'}{p_6}\right)^{\frac{\gamma-1}{\gamma}} - 1}{\sin \alpha_6}\right]^2\right\}^{\frac{1}{2}}$$

3178

3178

where $T_7'$ is the arithmetic average of total temperatures obtained from the thermocouple rake at station 7. The outlet total pressure was calculated at station 6 by assuming that there is no change in total temperature between stations 6 and 7. This assumption was made in the belief that a more reliable indication of total temperature could be obtained at station 7 because (1) the fluctuations of the gas flow would have more time to dampen out, (2) the gas velocity would be considerably lower, and (3) there is little heat transfer between the two stations.

The turbine efficiency was calculated as a ratio of the actual enthalpy drop as obtained from torque, weight-flow, and rotor-speed measurements to the ideal enthalpy drop as obtained from the inlet total temperature and the calculated total-pressure ratio.

The precision of the measured and calculated parameters is estimated to be within the following limits:

| | |
|---|---|
| Temperature, $^{\circ}R$ | ±0.5 |
| Pressure, in. Hg | ±0.05 |
| Turbine speed, percent | ±0.5 |
| Torque, percent of design | ±0.5 |

## RESULTS AND DISCUSSION

### Stator Weight-Flow Check

Before the performance of the transonic turbine was obtained, a stator weight-flow check was made without the rotor in place. It was found that at design stator total-to-static pressure ratio a weight flow $1\frac{1}{2}$ percent less than design was passed. The stator throat area was accordingly increased so that design weight flow could be passed in the performance investigation. As discussed in the previous section, a 3-percent total-pressure loss was assumed to occur (effectively this is a 0.97 flow coefficient). The decrease in weight flow from design obtained in the weight-flow check could in part be caused by a total-pressure loss or boundary-layer growth greater than those assumed in the design. However, it was also found in a subsequent unpublished analysis that the

stator throat area obtained by the design procedure outlined previously in the section Stator Design was approximately 1 percent less than the throat area required to pass the same weight flow by satisfying the requirement of simple radial equilibrium across the stator throat from hub to tip. Thus, it is indicated that for choked-flow stators an improved stator design procedure would be one in which the requirement of simple radial equilibrium across the throat as well as in the free stream is included.



This result represents an extension of the results presented in reference 9, in which the effect of curved inner walls on the three-dimensional flow characteristics of the stator was considered.

## Over-All Performance Investigation

The over-all performance of the transonic turbine is presented in figure 9(a). The equivalent specific-work output $\Delta h'/\theta_{cr}$ is shown as a function of the weight flow - speed parameter $\epsilon w\sqrt{\theta}/\delta$ with rating total-pressure ratio, $p_0'/p_{6,x}'$, percent design speed, and adiabatic efficiency shown as contours. Design equivalent specific-work output was obtained at design equivalent speed with an adiabatic efficiency of 0.84, and a weight flow - speed parameter corresponding to the design value indicated that design specific weight flow was passed. Efficiencies of over 80 percent were also found to occur over a considerable range of performance with the decrease in efficiency at lower speeds being comparable with that of more conservative turbine designs. It can also be noted that at design equivalent speed the specific-work output at the turbine limiting-loading point (23.3 Btu/lb) is only 3 percent above design specific-work output (22.6 Btu/lb). This proximity of the design point to the turbine limiting-loading point not only indicates the critical nature of high Mach number turbines but checks closely with the prediction of the design point being 5 percent below the limiting-loading point. From these results it can be concluded that the quasi-three-dimensional design procedure developed in this report and used in this transonic turbine-rotor design was sufficiently rigorous that the turbine design requirements, although very critical in nature, could be met.

As indicated by figure 9(a), the maximum value of adiabatic efficiency obtained was 0.85 and occurred at high pressure ratios and at speeds greater than design. As discussed previously in this section, this efficiency is based on the axial component of total-pressure ratio. A better evaluation of the turbine aerodynamic performance can be made by using the actual total-pressure ratio as a basis. The performance

map obtained on this basis is shown in figure 9(b). The region of 0.85 efficiency is again noted at speeds greater than design, thus indicating that zero exit whirl occurs at the increased speeds. The efficiency on this basis is also seen to be approximately 0.85 at the design point. Thus one point in the rating efficiency is lost as an exit-whirl loss. As pointed out in the section TURBINE DESIGN, the turbine was designed for this condition.

## Survey Investigation



In order to obtain an insight as to the loss characteristics of high Mach number turbines, detailed radial and circumferential surveys were made downstream of the transonic turbine stator and rotor at approximately the design point. The results of these surveys are shown in figure 10. The results of the stator-exit surveys are presented in figure 10(a) in terms of measured total-pressure ratio across the stator, whereas the results of the rotor surveys (fig. 10(b)) are shown in terms of the blade-element adiabatic efficiency across the turbine from stator inlet to rotor exit. It should be noted that the results presented in figure 10 serve only to indicate general trends in total pressures and blade-element efficiencies over approximately one stator pitch, and the numbers shown are not necessarily representative of the actual level. This is so because probe recovery was not considered downstream of the stator. Also gas fluctuations downstream of the rotor and instrument recording errors are sources of deviation from the actual case.

In figure 10(a) large cores are seen to be eminating from the turbine-stator hub. As indicated by reference 10, these cores are caused by secondary flows within the stator and they become very large as the stator-exit Mach numbers are increased to values corresponding with those used in the transonic turbine. The effect of these high loss cores on turbine efficiency is indicated by the results of the rotor-exit surveys presented in figure 10(b). Near the hub a small region of relatively low efficiency is seen. This region was observed to occur at intervals corresponding to one stator pitch, indicating that the low efficiency in this region was a result of the stator cores passing through the rotor. Since there is no band of low efficiency near the hub, it can be concluded that the high design rotor-entrance Mach numbers did not appreciably affect losses within the rotor. Large regions of low efficiencies near the tip can also be noted. Secondary-flow phenomena such as passage, tip clearance, and scraping vortices (see ref. 11) as well as the diffusion across the blade can contribute to the losses near the tip. From these results it is evident that the loss patterns for the transonic turbine are quite similar to the loss patterns for lower Mach number turbines, with the higher Mach number level probably giving rise to increased secondary-flow losses.

## SUMMARY OF RESULTS

The design and experimental investigation of a transonic turbine are presented herein. The turbine was designed for a slight amount of negative reaction and a limiting rotor-blade-surface Mach number of 1.33. The design procedure used was on a quasi-three-dimensional basis. The pertinent results of the investigation can be summarized as follows:



1. At design speed, design equivalent weight flow was passed and design equivalent specific-work output was obtained at an adiabatic efficiency (based on total-pressure ratio with the axial component of velocity at the turbine exit) of 0.84. The adiabatic efficiency for the preceding condition but based on actual total-pressure ratio was 0.85, which was the highest efficiency obtained over the range of the performance investigated. Design specific-work output was only 3 percent below the turbine limiting-loading point. This checked closely with the prediction of the design point being 5 percent below the limiting-loading point.

2. Efficiencies of over 0.80 were found to occur over a considerable range of performance with the decrease in efficiency at lower speeds being comparable with that associated with more conservative turbine designs.

3. The loss patterns obtained from surveys behind both the stator and rotor at approximately the design point were found to be quite similar to the loss patterns for lower Mach number turbines, with the higher Mach number level of the transonic turbine probably giving rise to increased secondary-flow losses within the stator and rotor. Large losses at the rotor-tip exit were found to occur and are probably caused by adverse secondary-flow effects within the rotor.

## CONCLUSIONS

From the results of the experimental investigation of the transonic turbine, it can be concluded that high Mach number turbines utilizing rotor-hub entrance Mach numbers of unity can be obtained with efficiencies of at least 85 percent under the prescribed conditions of surface Mach number and reaction. It can also be concluded that the quasi-three-dimensional design procedure used was sufficiently rigorous that, although the turbine was designed to operate extremely close to the limiting-loading point, this design condition was met satisfactorily.

Lewis Flight Propulsion Laboratory
National Advisory Committee for Aeronautics
Cleveland, Ohio, December 11, 1953

## APPENDIX A

## SYMBOLS

The following symbols are used in this report:

| | |
|---|---|
| A | area, sq ft |
| $A_{cr}/A$ | ratio of area required at Mach number of unity to required area at specified Mach number |
| C | blade-surface curvature, 1/ft |
| g | acceleration due to gravity, 32.17 $ft/sec^2$ |
| $\Delta h$ | specific enthalpy drop, Btu/lb |
| N | rotative speed, rpm |
| n | orthogonal length, ft |
| o | blade-throat dimension, ft |
| p | absolute pressure, lb/sq ft |
| R | gas constant |
| r | radius, ft |
| s | blade spacing, ft |
| T | total temperature, $^{\circ}F$ abs |
| t | blade thickness in tangential direction, ft |
| U | blade velocity, ft/sec |
| V | absolute gas velocity, ft/sec |
| W | relative gas velocity, ft/sec |
| w | weight flow, lb/sec |
| y | distance along orthogonal in radial-axial plane, ft |
| $\alpha$ | absolute gas flow angle measured from tangential direction |
| $\beta$ | relative gas flow angle into and out of rotor measured from axial direction |

3178

$\gamma$ ratio of specific heats

$\delta$ ratio of inlet-air total pressure to NACA standard sea-level pressure, $p_0'/p^*$

$\epsilon$ function of $\gamma$, $\frac{\gamma^*}{\gamma}\left[\frac{\left(\frac{\gamma+1}{2}\right)^{\frac{\gamma}{\gamma-1}}}{\left(\frac{\gamma^*+1}{2}\right)^{\frac{\gamma^*}{\gamma^*-1}}}\right]$

$\eta$ adiabatic efficiency defined as ratio of turbine work based on torque, weight flow, and speed measurements to ideal work based on inlet total temperature, and inlet and outlet total pressure, both defined as sum of static pressure plus pressure corresponding to gas velocity

$\eta_e$ blade-element adiabatic efficiency based on total-stage measurements upstream of stator and downstream of rotor

$\eta_x$ adiabatic efficiency defined as ratio of turbine work based on torque, weight flow, and speed measurements to ideal work based on inlet total temperature, and inlet and outlet total pressure, both defined as sum of static pressure plus pressure corresponding to axial component of velocity

$\theta_{cr}$ squared ratio of critical velocity at turbine inlet to critical velocity at NACA standard sea-level temperature, $(V_{cr}/V_{cr}^*)^2$

$\rho$ gas density, lb/cu ft

$\varphi$ blade mean camber angle, measured from axial direction

$\omega$ angular speed, radians/sec

Subscripts:

a annulus area

cr conditions at Mach number of unity

h hub

m midchannel

p pressure surface

s suction surface

t tip

te trailing edge

x axial direction

0 station upstream of stator (see fig. 7)

1 station at throat of stator passage

2 station at outlet of stator just upstream from trailing edge

3 station at free-stream condition between stator and rotor

4 station at throat of rotor passage

5 station at outlet of rotor just upstream from trailing edge

6 station downstream from turbine

7 station 4 feet downstream from rotor

Superscripts:

* NACA standard conditions

' total state

## APPENDIX B

## CALCULATION METHODS

The following discussion presents equations and methods used in obtaining the surface velocity distribution, the midchannel velocity distribution, and the weight flow through the transonic turbine rotor.

### Surface Velocity Distribution

For a given midchannel velocity distribution, the suction- and pressure-surface velocities were obtained by using figures 11(a) and (b), which are reprints of figures 17 and 18, respectively, in reference 7. The main assumption made in obtaining these figures was that the curvature on the channel orthogonal varied linearly from suction to pressure surface. With reference to figure 3 the assumption was made that the center of the channel orthogonal determined the axial position of the orthogonal for use in conjunction with the axial symmetric analysis. For a trial blade shape, a series of channel orthogonals are drawn (typical ones shown in fig. 3). The curvatures $C_s$ and $C_p$ are obtained by use of a radometer (see appendix C of ref. 12 for description), and the orthogonal length n is measured. The parameters in figure 11 are calculated from these quantities, and the ratio of the suction-surface and pressure-surface velocities to the midchannel velocities can be obtained. Then for a known or assumed midchannel velocity distribution, the surface velocities can be computed.

### Midchannel Velocity Distribution

The midchannel velocity distribution was obtained by using a simplification of the method presented in reference 12. The assumptions made in obtaining the midchannel velocity distribution for the transonic turbine are:

(1) An axial symmetric condition exists.

(2) The streamline shift in the radial direction is small enough that the axial symmetric orthogonal can be assumed to be a radial line (see fig. 3).

(3) The flow is assumed to follow the blade mean camber angle $\varphi$ (fig. 3).

(4) Simple radial equilibrium exists.

[redacted]

Equation (3) of reference 12 was used to obtain the midchannel velocity distribution for the prescribed hub velocity. The equation rewritten here is

$$W = e^{\int_0^y a\,dy}\left(W_h - \int_0^y b\,e^{-\int_0^y a\,dy}\,dy\right) \qquad (B1)$$

where in view of the above assumptions

$$a = -\frac{\sin^2\varphi}{r}$$

$$b = 2\omega \sin\varphi$$

Thus with the geometry of the three sections known and the relative velocity at the hub assumed or prescribed, the relative velocity at any point within the blade passage can be calculated.

3178

## Weight Flow

Once the midchannel velocity distribution is known, the axial symmetric weight flow that passes the radial-axial orthogonal can be obtained from the equation

$$w = 2\pi \int_{r_h}^{r_t} \rho W \cos\varphi \left(1 - \frac{t}{s}\right) r\,dr$$

Because the velocity across the channel varies from the midchannel velocity distribution, the weight flow was then adjusted in the following manner: Figure 12 shows the ratio of specific-flow area at a given $W/W_{cr}$ to that corresponding to $W/W_{cr} = 1$ as a function of $W/W_{cr}$. For a given $W/W_{cr}$ at midchannel (shown in fig. 12), area ABCD would represent the area that would be used in the calculation of the axial symmetric weight flow. The area AEFD is the area required to pass that weight flow including the variation in velocity across the channel when linear variation in velocity is assumed. The ratio of the areas AEFD/ABCD was obtained at the three sections for a given axial symmetric orthogonal and was averaged. The axial symmetric weight flow was then increased by the average ratio and this weight flow compared with the design value. It is recognized that other assumptions, such as a linear variation in streamline curvature as suggested in reference 7 or a linear variation in static pressure, may be closer to the actual case. However, differences in the blade shapes resulting from the various assumptions are slight and, as borne out by the experimental investigation, the assumption of linear variation in velocity was sufficiently accurate.

REFERENCES

1. Cohen, Leo: Theoretical Investigation of Velocity Diagrams of a Single-Stage Turbine for a Turbojet Engine at Maximum Thrust Per Square Foot Turbine Frontal Area. NACA TN 2732, 1952.

2. Klapproth, John F.: General Considerations of Mach Number Effects on Compressor-Blade Design. NACA RM E53L23a, 1954.

3. The Staff of the Ames 1- by 3-Foot Supersonic Wind-Tunnel Section: Notes and Tables for Use in the Analysis of Supersonic Flow. NACA TN 1428, 1947.

4. Hauser, Cavour H., and Plohr, Henry W.: Two-Dimensional Cascade Investigation of the Maximum Exit Tangential Velocity Component and Other Flow Conditions at the Exit of Several Turbine Blade Designs at Supercritical Pressure Ratios. NACA RM E51F12, 1951.

5. Stewart, Warner L., Schum, Harold J., and Whitney, Warren J.: Investigation of Turbines for Driving Supersonic Compressors. I - Design and Performance of First Configuration. NACA RM E52C25, 1952.

6. Whitney, Warren J., Stewart, Warner L., and Schum, Harold J.: Investigation of Turbines for Driving Supersonic Compressors. IV - Design and Performance of Second Configuration Including Study of Three-Dimensional Flow Effects. NACA RM E53C02, 1953.

7. Huppert, M. C., and MacGregor, Charles: Comparison Between Predicted and Observed Performance of Gas-Turbine Stator Blade Designed for Free-Vortex Flow. NACA TN 1810, 1949.

8. Rebeske, John J., Jr.: Investigation of a NACA High Speed Strain-Gage Torquemeter. NACA TN 2003, 1950.

9. Stewart, Warner L., Whitney, Warren J., and Heaton, Thomas R.: Effect of Certain Combinations of Wall Contouring and Design Exit Velocity Distribution on Prediction of Turbine-Nozzle Mass Flow. NACA RM E53E14, 1953.

10. Rohlik, Harold E., Allen, Hubert W., and Herzig, Howard Z.: Study of Secondary-Flow Patterns in an Annular Cascade of Turbine Nozzle Blades with Vortex Design. NACA TN 2909, 1953.

11. Hansen, Arthur G., Herzig, Howard Z., and Costello, George R.: A Visualization Study of Secondary Flows in Cascades. NACA TN 2947, 1953.

12. Stewart, Warner L.: Analytical Investigation of Flow Through a High-Speed Mixed-Flow Turbine. NACA RM E51H06, 1951.

TABLE I. - STATOR-BLADE-SECTION COORDINATES

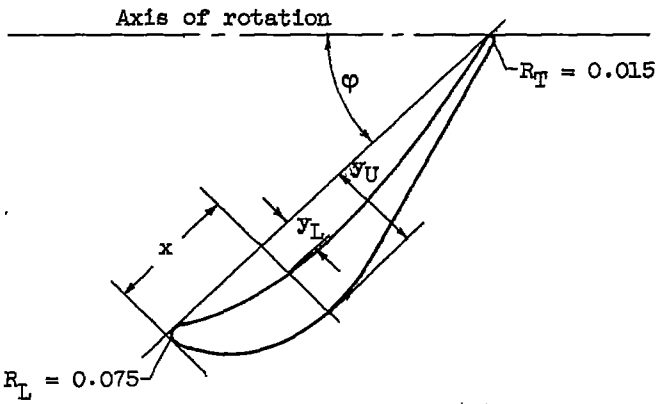


| x | Hub | | Mean | | Tip | |
|---|---|---|---|---|---|---|
| | φ, deg | | | | | |
| | 40.5 | | 44.9 | | 50.1 | |
| | $r/r_t$ | | | | | |
| | 0.70 | | 0.85 | | 1.00 | |
| | $y_L$ | $y_U$ | $y_L$ | $y_U$ | $y_L$ | $y_U$ |
| 0 | 0.075 | 0.075 | 0.075 | 0.075 | 0.075 | 0.075 |
| .100 | .004 | .226 | .004 | .224 | .005 | .228 |
| .200 | .076 | .294 | .061 | .300 | .059 | .313 |
| .300 | .131 | .335 | .110 | .349 | .107 | .370 |
| .400 | .169 | .358 | .149 | .378 | .145 | .411 |
| .500 | .194 | .367 | .179 | .393 | .177 | .437 |
| .600 | .209 | .364 | .201 | .397 | .201 | .450 |
| .700 | .217 | .351 | .215 | .391 | .219 | .452 |
| .800 | .217 | .331 | .223 | .378 | .231 | .445 |
| .900 | .217 | .305 | .225 | .358 | .239 | .431 |
| 1.000 | .201 | .276 | .222 | .333 | .242 | .409 |
| 1.100 | .185 | .246 | .214 | .306 | .240 | .384 |
| 1.200 | .166 | .215 | .202 | Straight line | .235 | .355 |
| 1.300 | .142 | Straight line | .186 | | .226 | .326 |
| 1.400 | .116 | | .167 | | .215 | Straight line |
| 1.500 | .088 | | .145 | | .200 | |
| 1.600 | .060 | | .121 | | .182 | |
| 1.700 | .031 | | .096 | | .161 | |
| 1.800 | .002 | | .070 | | .139 | |
| 1.813 | .001 | .028 | ----- | | ----- | |
| 1.824 | .015 | .015 | ----- | | ----- | |
| 1.850 | ----- | ----- | .056 | | .127 | |
| 2.000 | ----- | ----- | .015 | | .088 | |
| 2.050 | ----- | ----- | .005 | .031 | .075 | |
| 2.068 | ----- | ----- | .015 | .015 | ----- | |
| 2.250 | ----- | ----- | ----- | ----- | .018 | .047 |
| 2.327 | ----- | ----- | ----- | ----- | .015 | .015 |

3178

TABLE II. - ROTOR-BLADE-SECTION COORDINATES

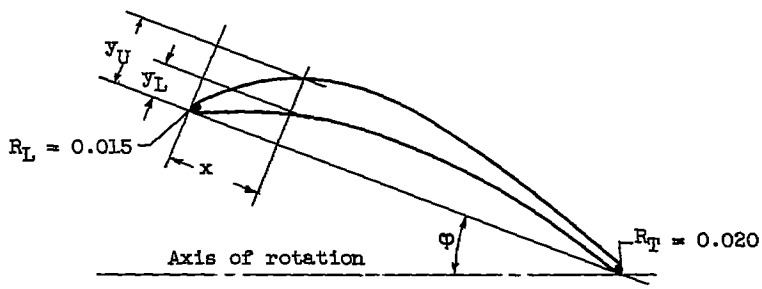


| x | Hub | | Mean | | Tip | |
|---|---|---|---|---|---|---|
| | φ, deg | | | | | |
| | -7.3 | | 8.8 | | 21.4 | |
| | $r/r_t$ | | | | | |
| | 0.70 | | 0.85 | | 1.00 | |
| | $y_L$ | $y_U$ | $y_L$ | $y_U$ | $y_L$ | $y_U$ |
| 0 | 0.015 | 0.015 | 0.015 | 0.015 | 0.015 | 0.015 |
| .100 | .066 | .138 | .070 | .150 | .053 | .127 |
| .200 | .142 | .254 | .146 | .278 | .110 | .232 |
| .300 | .211 | .362 | .213 | .396 | .157 | .320 |
| .400 | .272 | .458 | .270 | .498 | .195 | .392 |
| .500 | .326 | .540 | .318 | .581 | .226 | .451 |
| .600 | .373 | .610 | .358 | .647 | .252 | .498 |
| .700 | .414 | .670 | .392 | .697 | .273 | .534 |
| .800 | .450 | .721 | .420 | .733 | .290 | .561 |
| .900 | .481 | .764 | .443 | .758 | .304 | .580 |
| 1.000 | .508 | .800 | .462 | .774 | .315 | .593 |
| 1.100 | .531 | .829 | .476 | .782 | .324 | .600 |
| 1.200 | .550 | .851 | .485 | .784 | .330 | .602 |
| 1.300 | .564 | .866 | .490 | .780 | .334 | .600 |
| 1.400 | .574 | .874 | .490 | .770 | .336 | .593 |
| 1.500 | .580 | .876 | .486 | .754 | .336 | .583 |
| 1.600 | .581 | .872 | .478 | .732 | .333 | .569 |
| 1.700 | .578 | .862 | .467 | .705 | .328 | .552 |
| 1.800 | .570 | .846 | .452 | .673 | .321 | .532 |
| 1.900 | .557 | .824 | .433 | .637 | .312 | .509 |
| 2.000 | .539 | .796 | .411 | .596 | .300 | .483 |
| 2.100 | .516 | .761 | .385 | .551 | .286 | .454 |
| 2.200 | .487 | .718 | .355 | .502 | .270 | .422 |
| 2.300 | .453 | .667 | .321 | .449 | .252 | .387 |
| 2.400 | .413 | .607 | .284 | .393 | .231 | .349 |
| 2.500 | .367 | .538 | .243 | .334 | .208 | .310 |
| 2.600 | .315 | .459 | .198 | .274 | .183 | .270 |
| 2.700 | .256 | .371 | .150 | .214 | .156 | .230 |
| 2.800 | .189 | .278 | .198 | .154 | .126 | .190 |
| 2.900 | .113 | .182 | .042 | .094 | .094 | .150 |
| 3.000 | .028 | .086 | .020 | .020 | .060 | .110 |
| 3.056 | .020 | .020 | ----- | ----- | ----- | ----- |
| 3.100 | ----- | ----- | ----- | ----- | .023 | .070 |
| 3.188 | ----- | ----- | ----- | ----- | .020 | .020 |

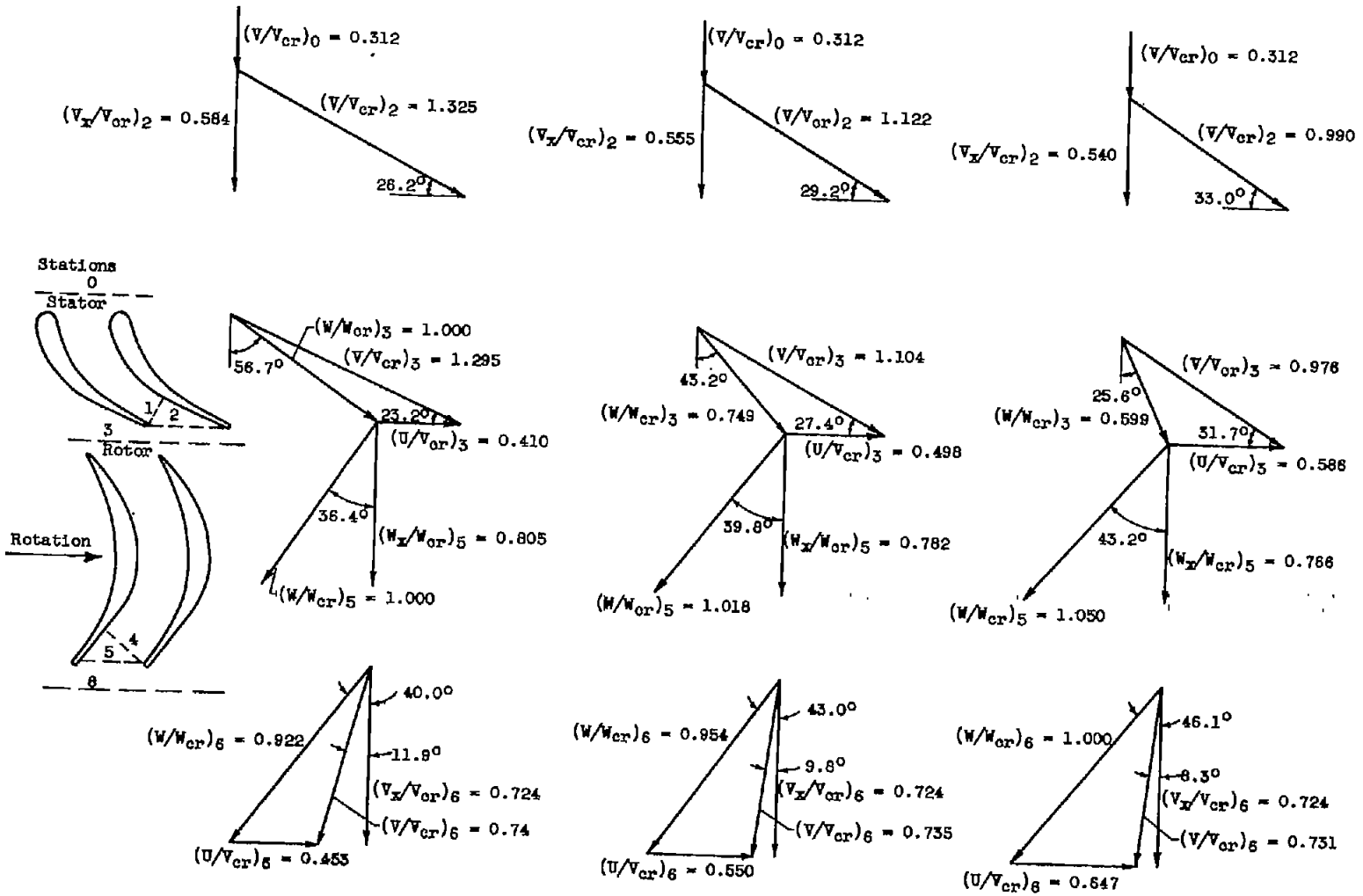


(a) Hub; $r/r_t$, 0.70.

(b) Mean; $r/r_t$, 0.85.

(c) Tip; $r/r_t$, 1.00.

Figure 1. - Transonic turbine velocity diagrams.

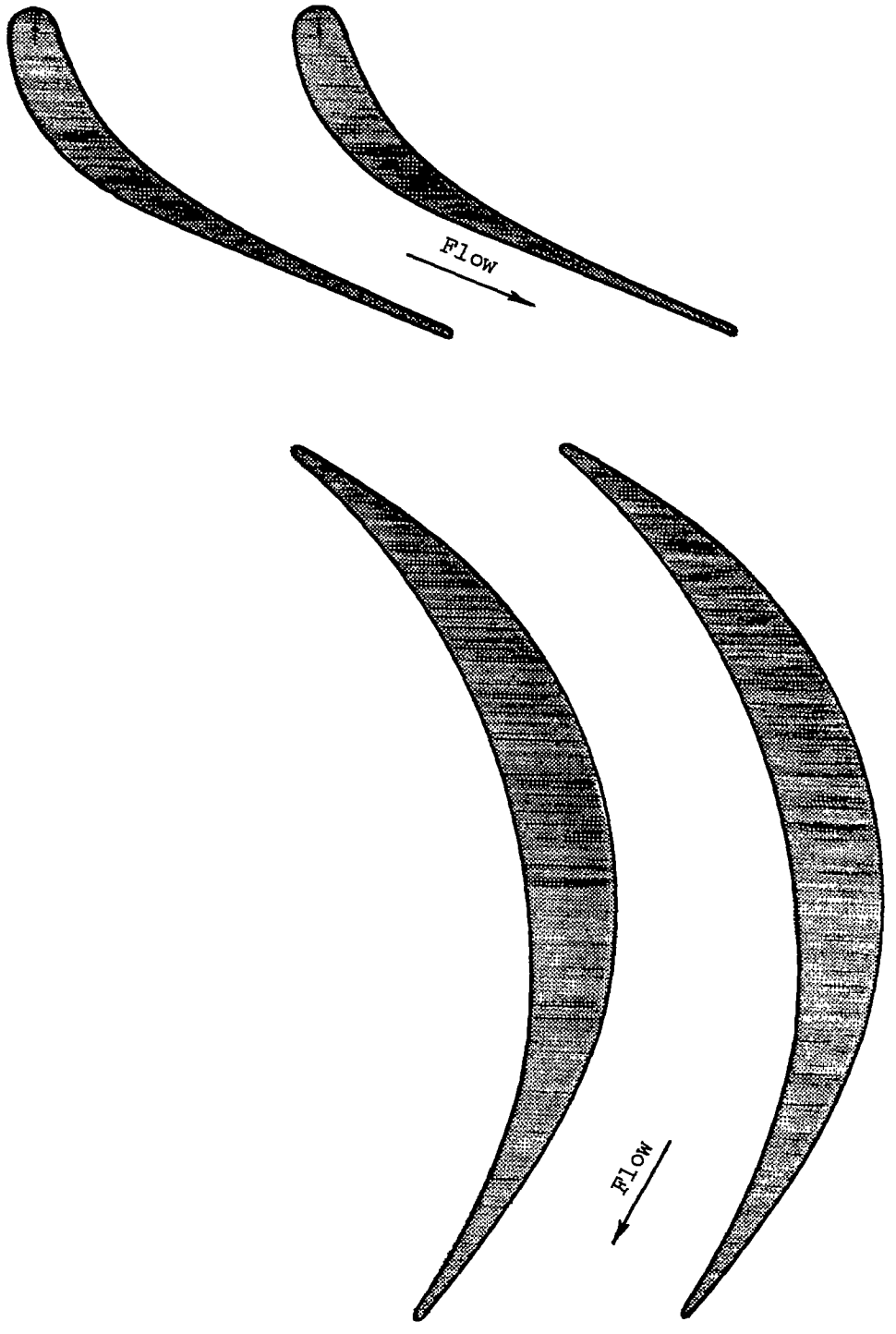


(a) Hub.

Figure 2. - Stator- and rotor-blade passages and profiles.

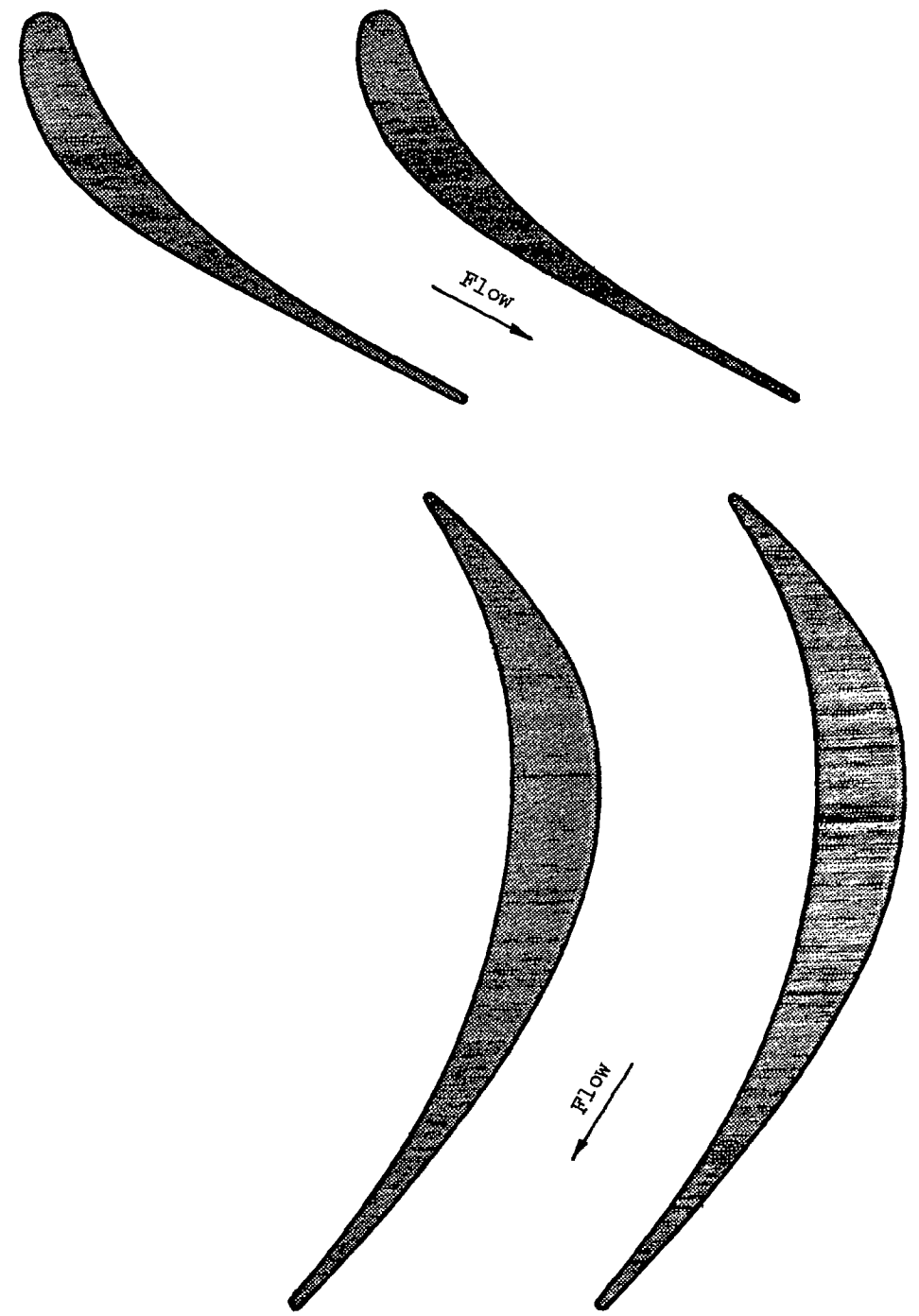


(b) Mean.

Figure 2. - Continued. Stator- and rotor-blade passages and profiles.

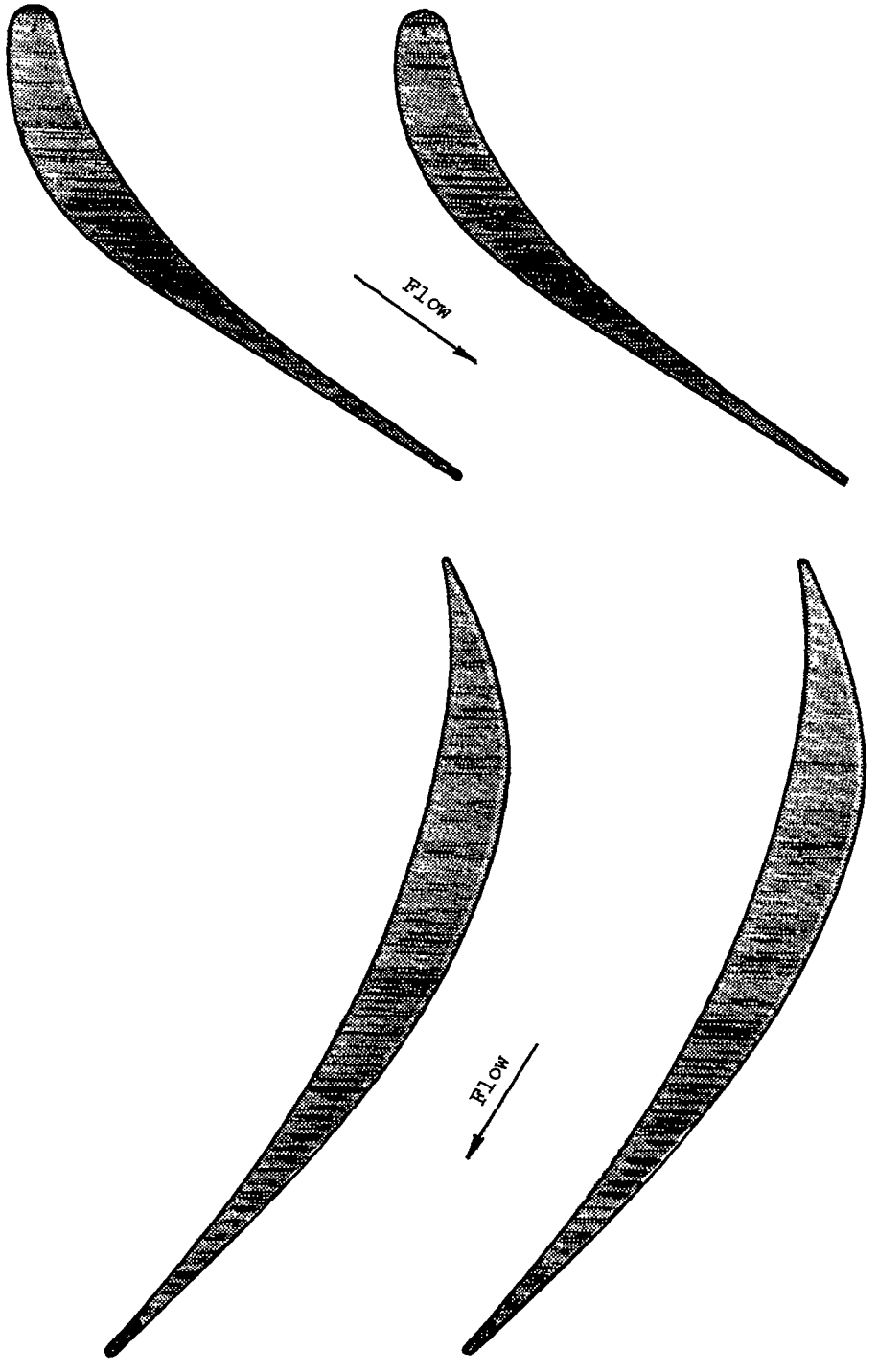


(c) Tip.

Figure 2. - Concluded. Stator- and rotor-blade passages and profiles.

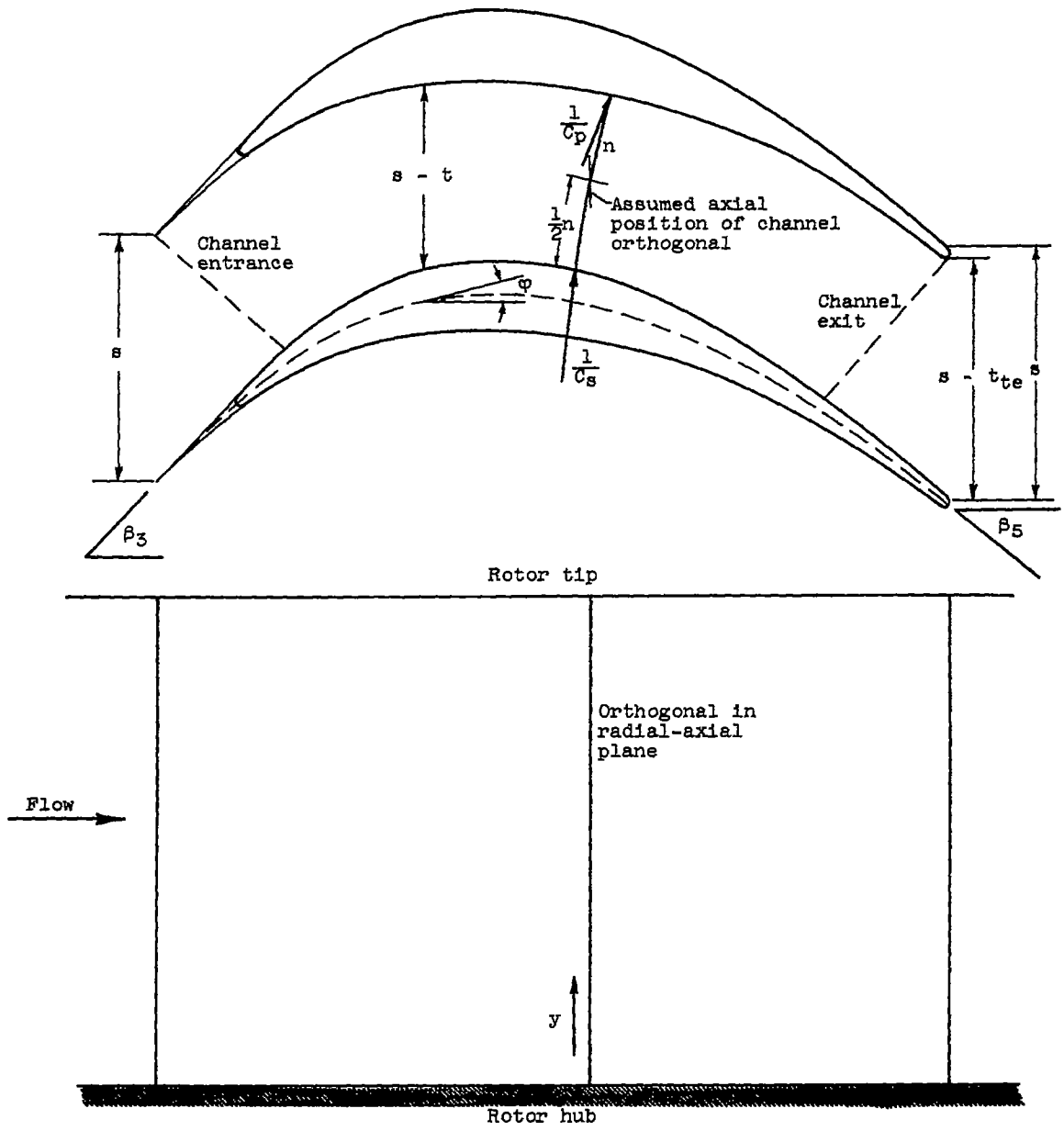


Figure 3. - Discription of variables involved in three-dimensional design procedure.

3178

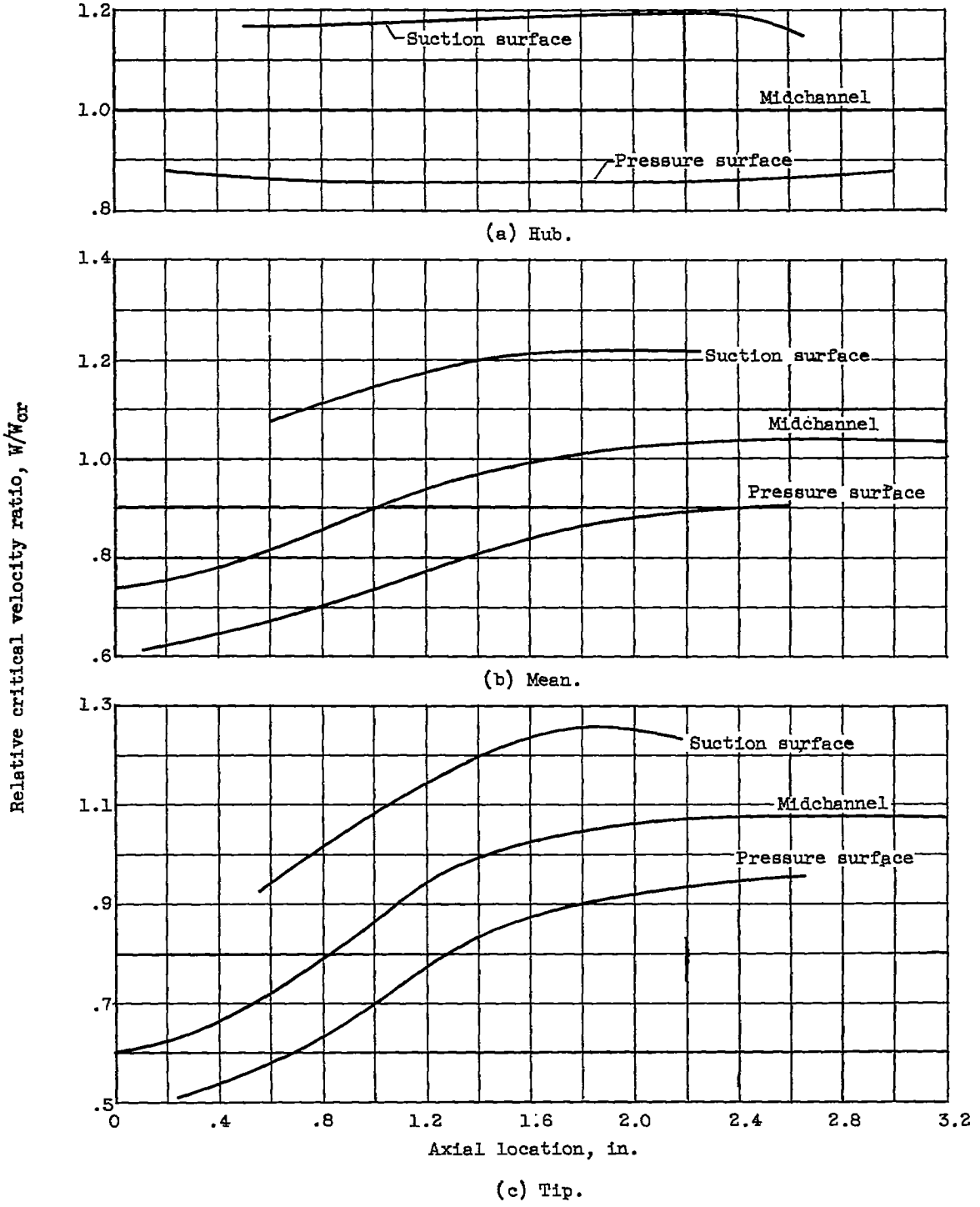


Figure 4. - Design rotor midchannel and surface velocity distributions at hub, mean, and tip sections.

[redacted]

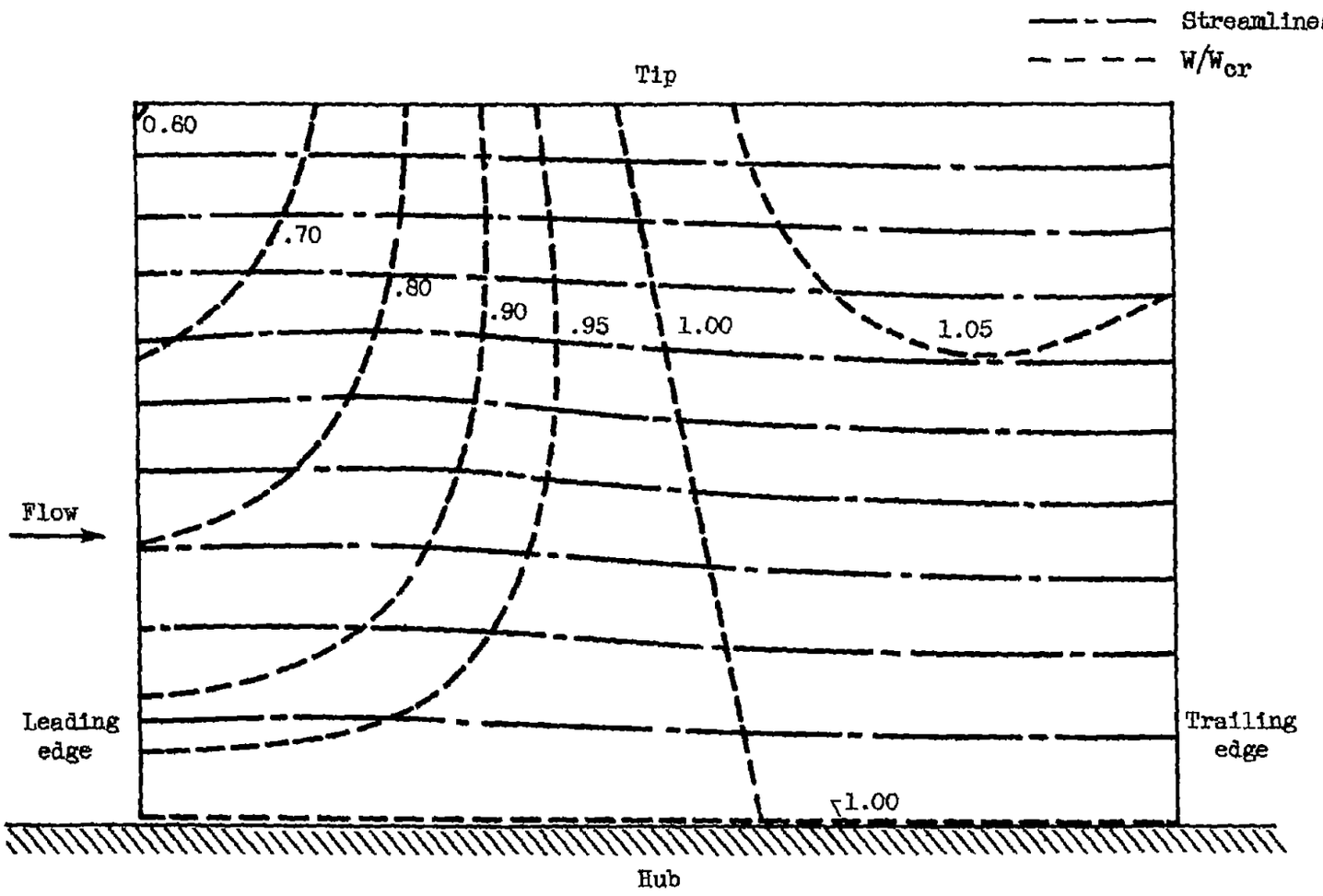


Figure 5. - Side view of transonic turbine rotor in radial-axial plane indicating design streamlines and velocity distributions.

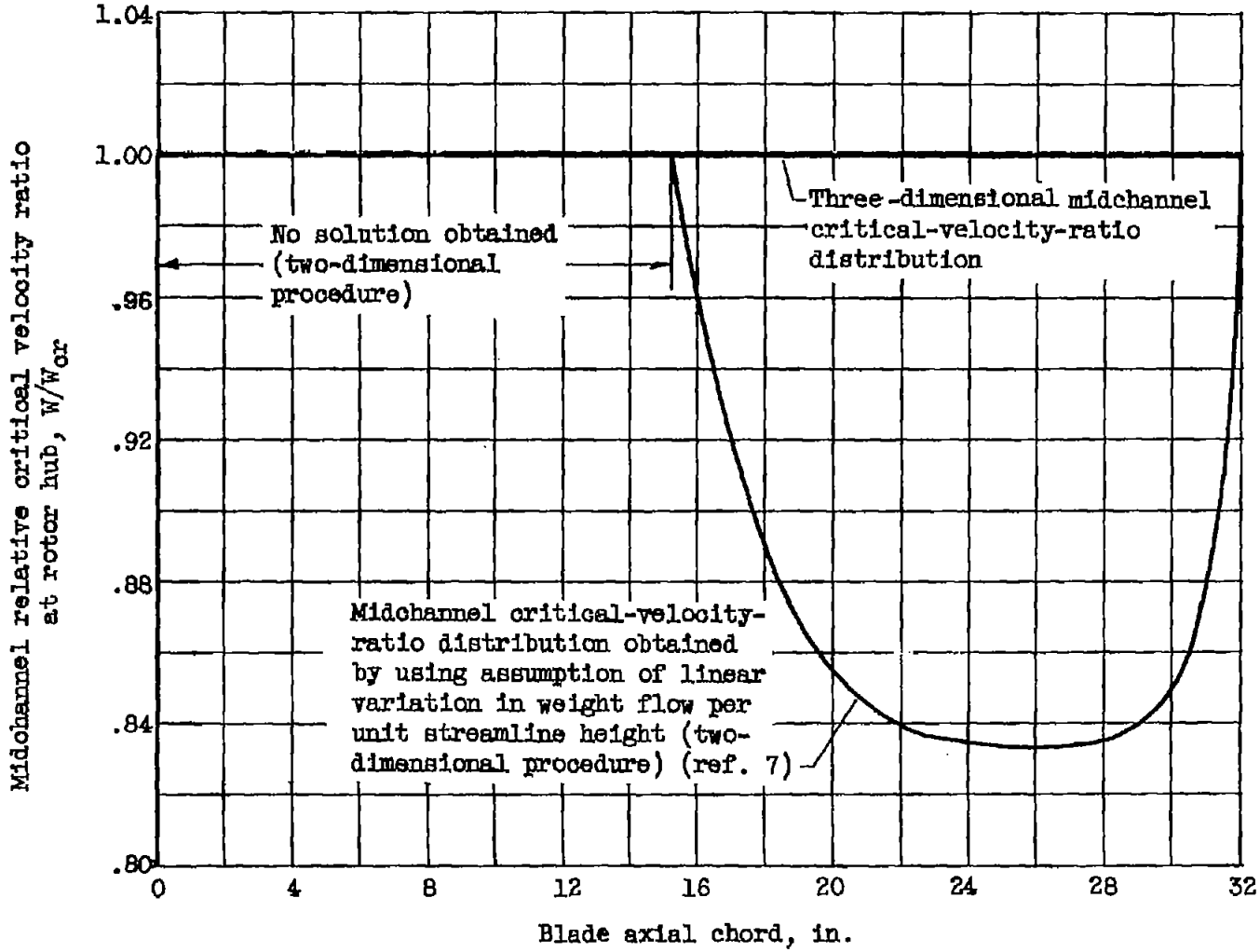


Figure 6. - Comparison of midchannel critical-velocity-ratio distributions across transonic-turbine-rotor hub obtained by using two- and three-dimensional design procedures.

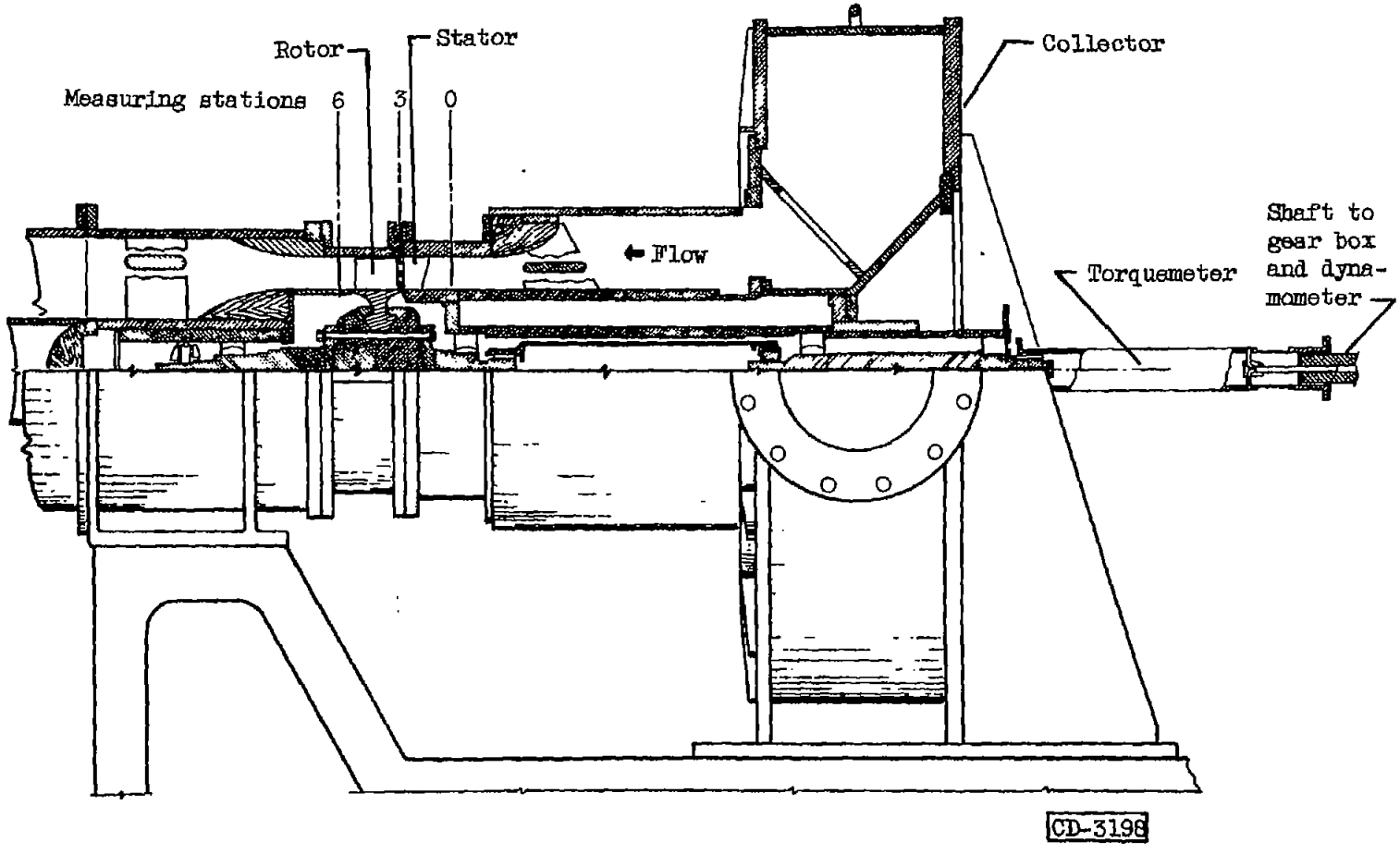


Figure 7. - Diagrammatic sketch of cold-air turbine test section.

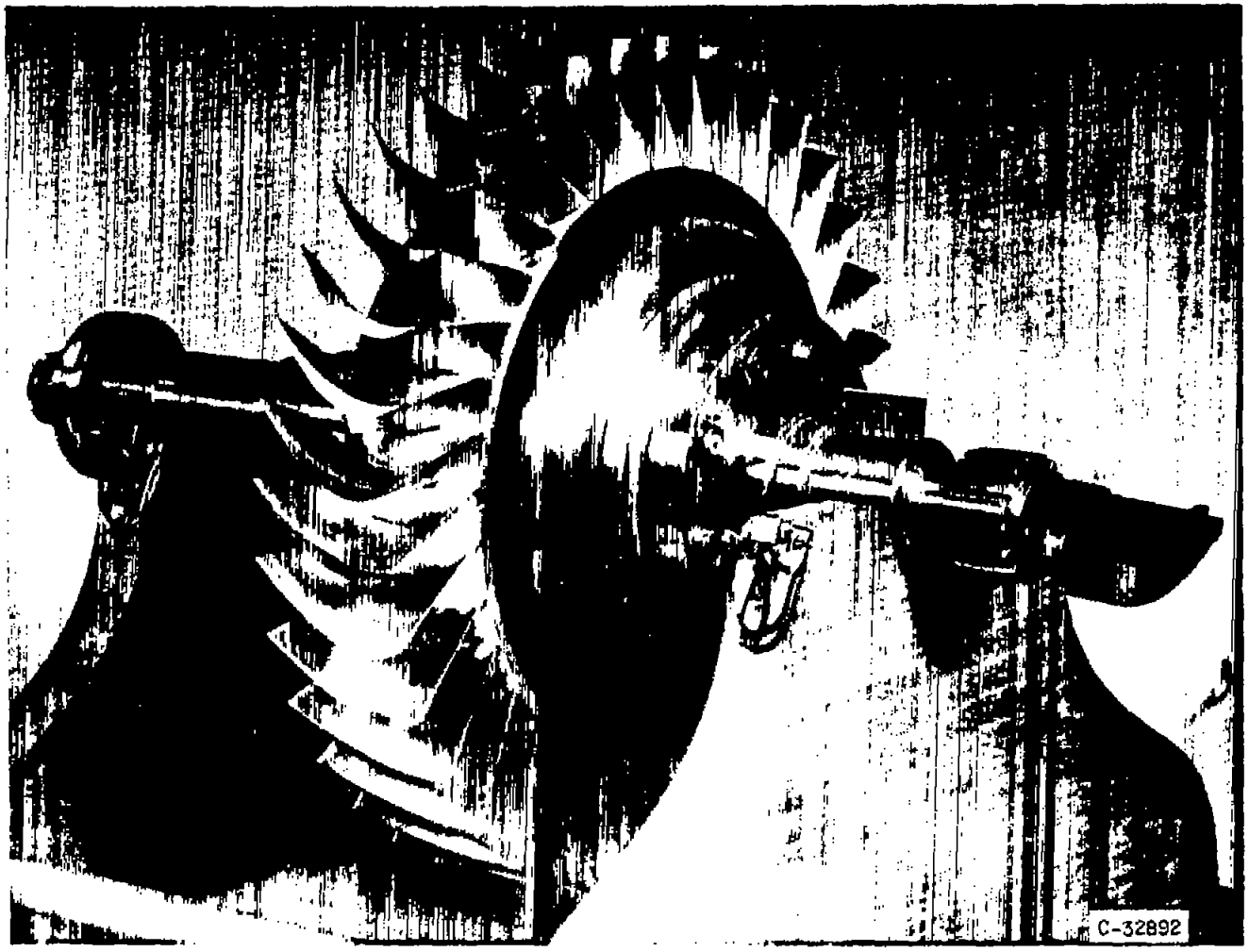


Figure 8. - Photograph of transonic turbine rotor.

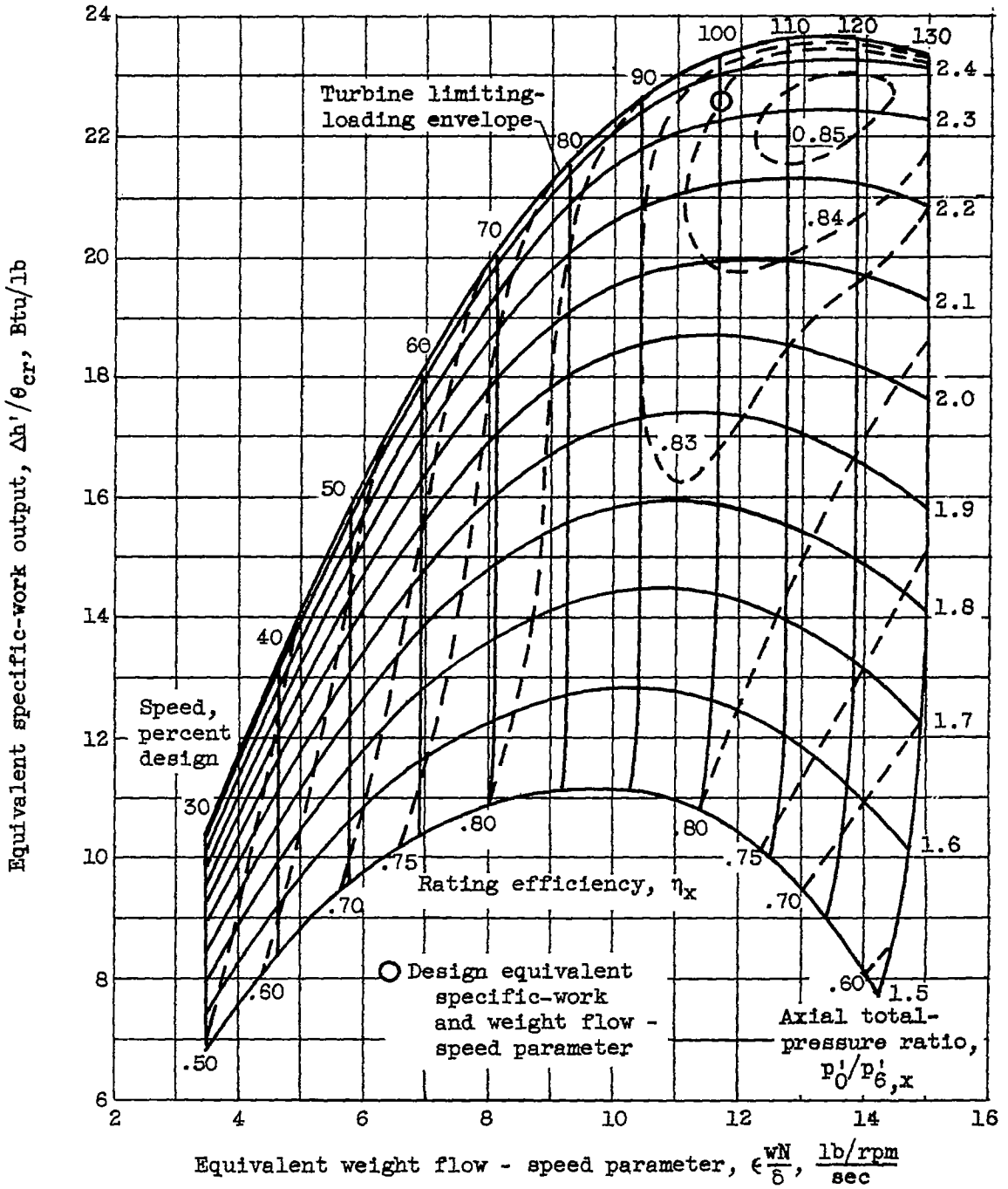


(a) Based on axial total-pressure ratio across turbine.

Figure 9. - Experimentally obtained performance map.

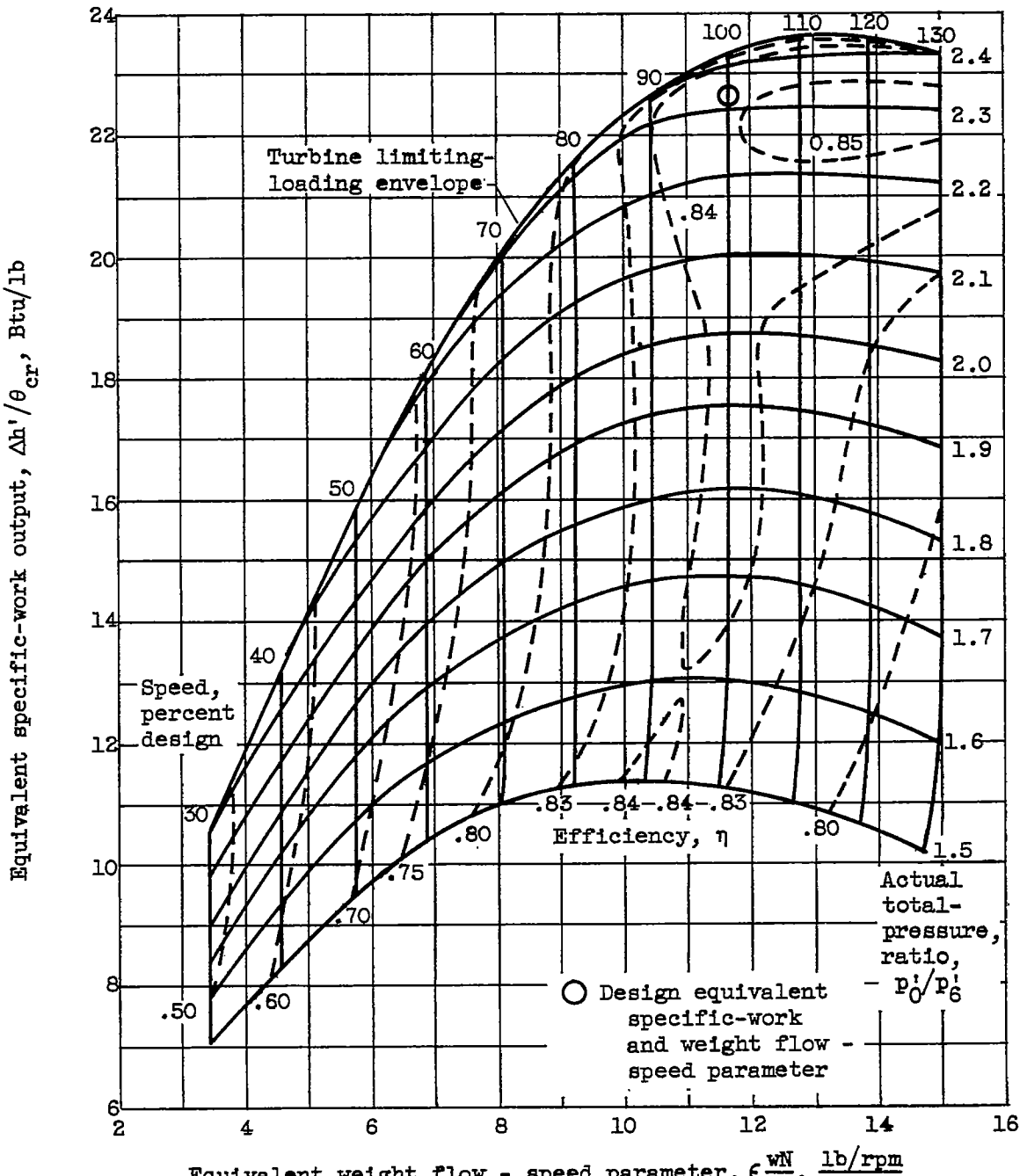


(b) Based on actual total-pressure ratio across turbine.

Figure 9. - Concluded. Experimentally obtained performance map.

[redacted]

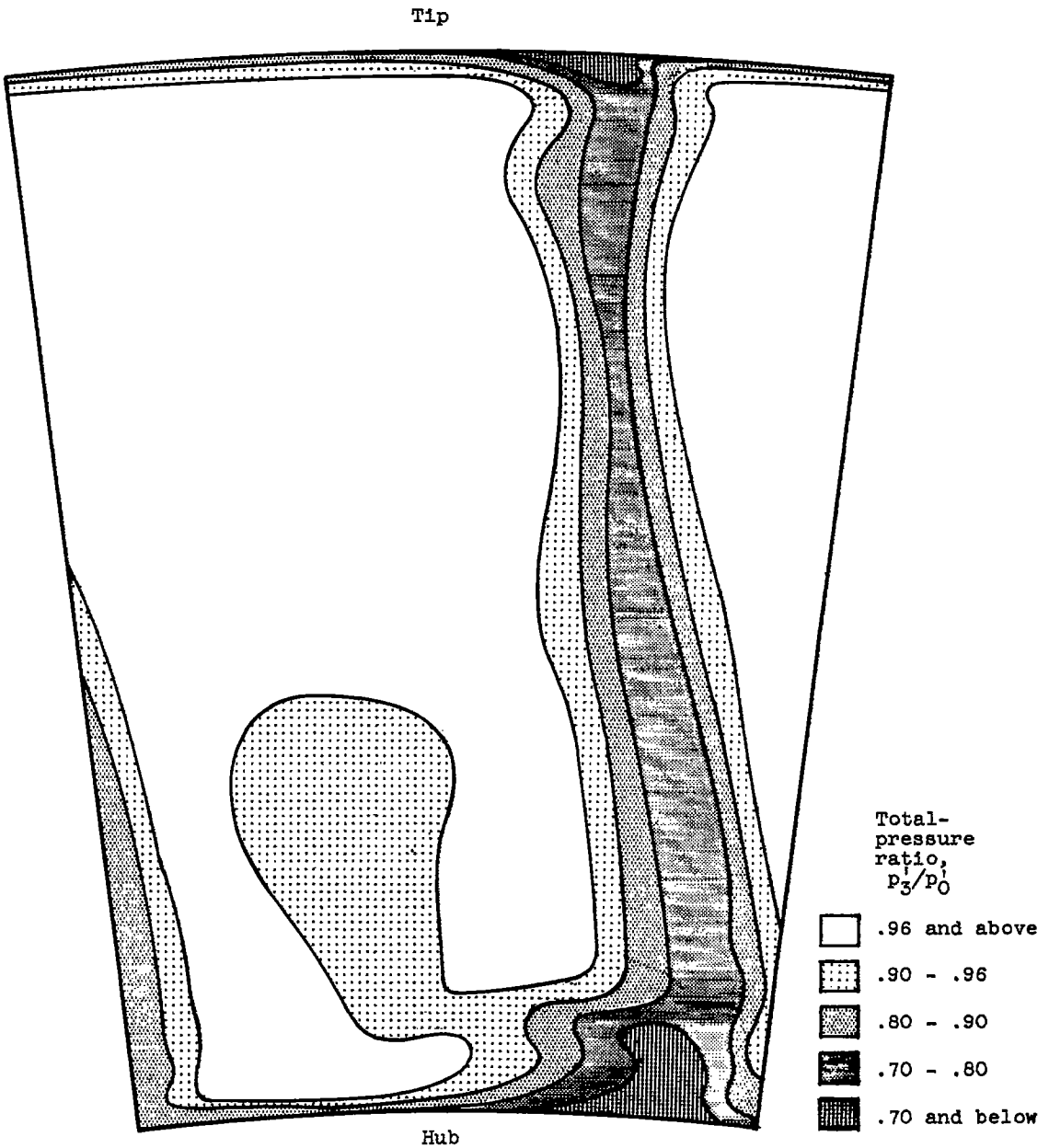


(a) Behind stator.

Figure 10. - Survey results at design point.

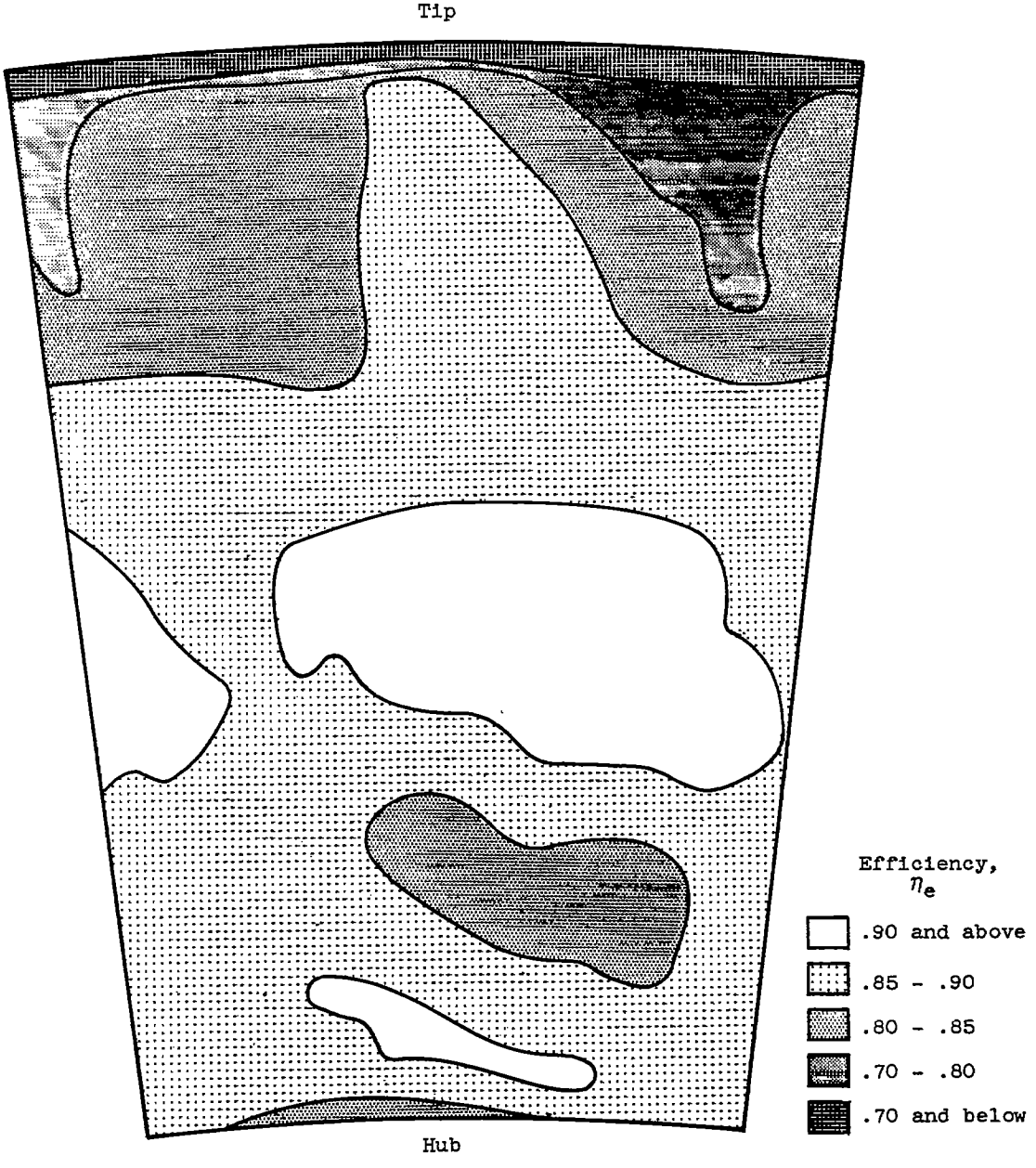


(b) Behind rotor.

Figure 10. - Concluded. Survey results at design point.

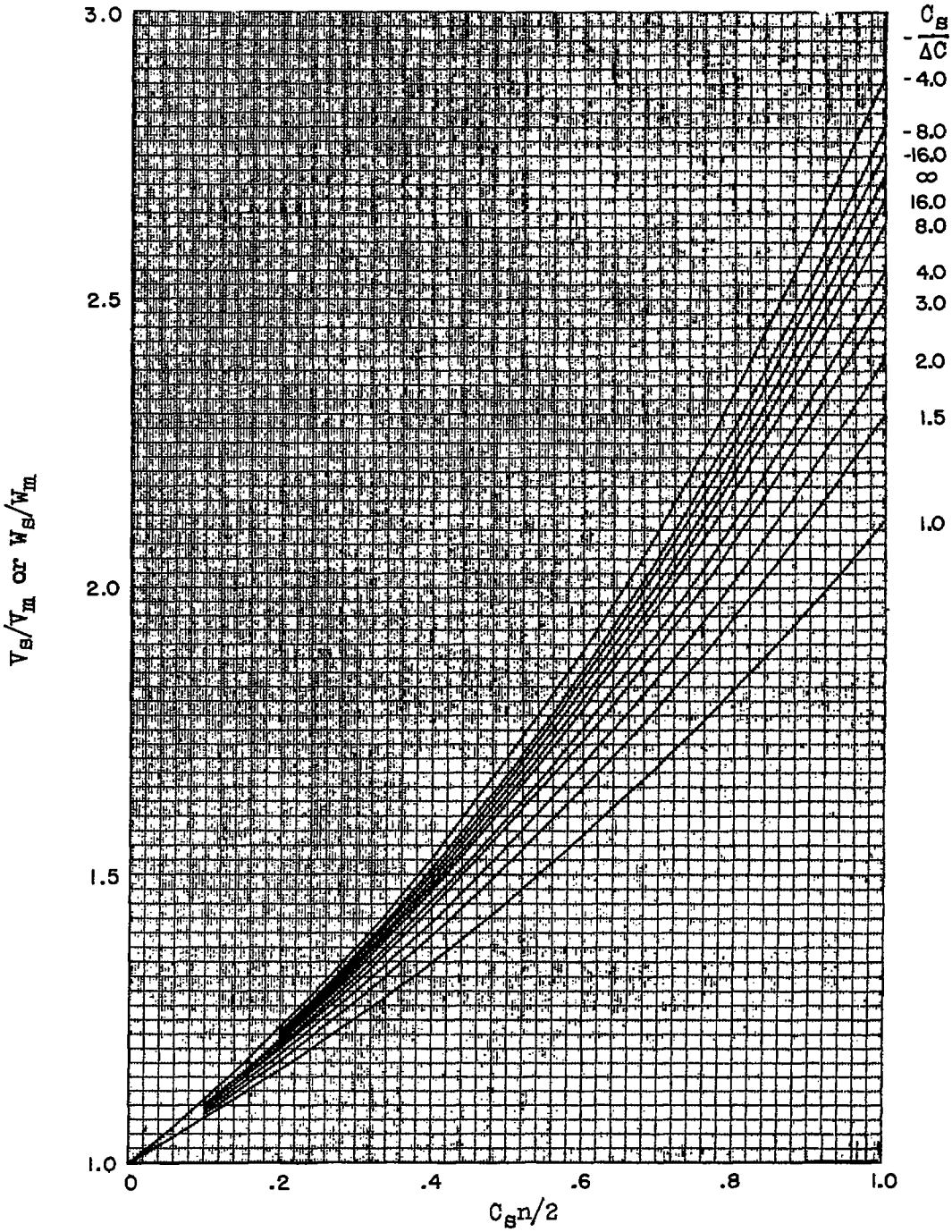


(a) Suction surface.

Figure 11. - Variation with channel width and blade curvature of ratio of velocities along blade surface to velocity at channel center. (Ref. 7, fig. 17.)

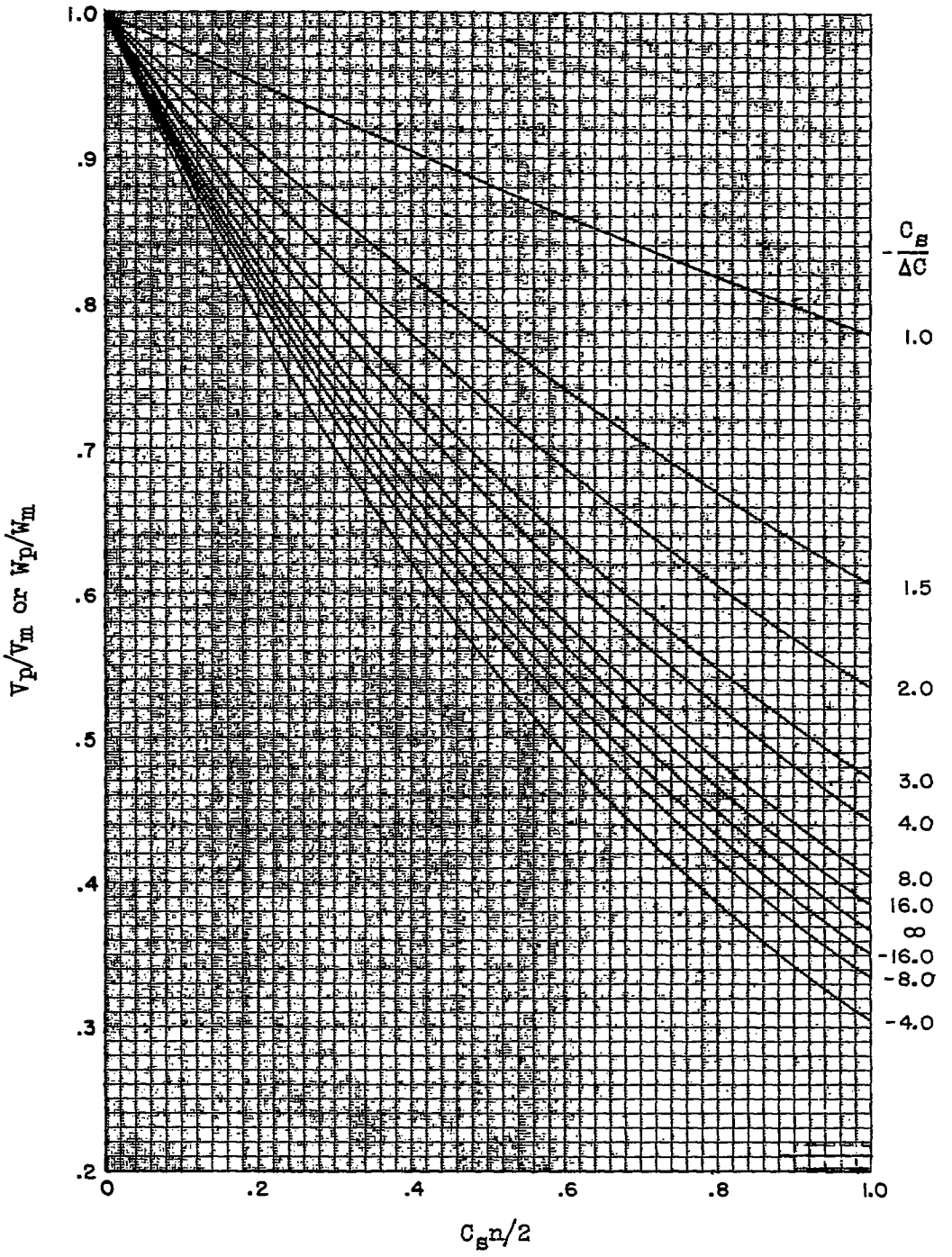


(b) Pressure surface.

Figure 11. - Concluded. Variation with channel width and blade curvature of ratio of velocities along blade surface to velocity of channel center. (Ref. 7, fig. 18.)

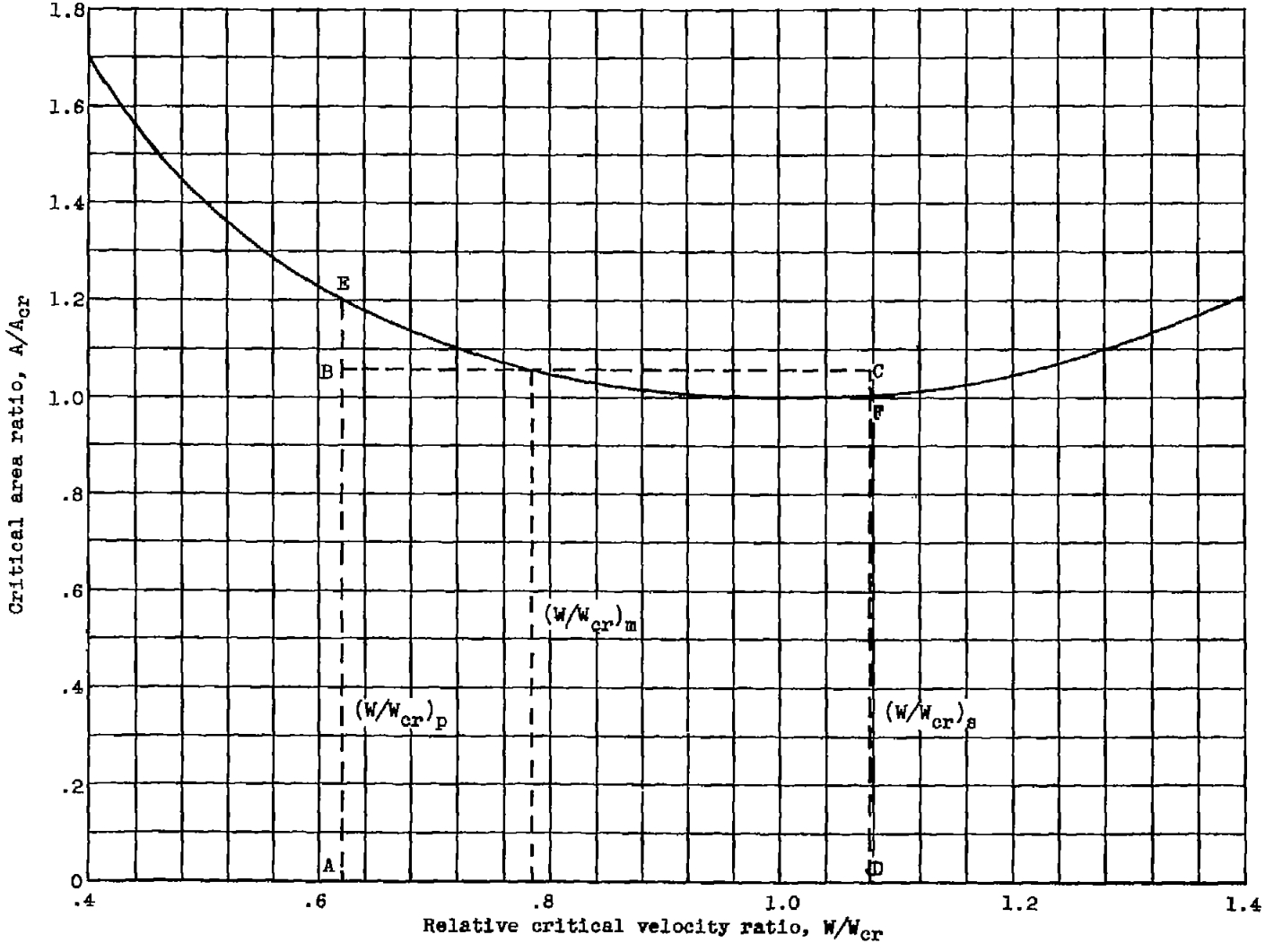


Figure 12. - Illustration of method of correcting calculated weight flow for velocity gradient from suction to pressure surface.